Contributions to Mineralogy and Petrology (2023) 178:26
https://doi.org/10.1007/s00410-023-02003-1

ORIGINAL PAPER

Primary cordierite with > 2.5 wt% CO_2 from the UHT Bakhuis Granulite Belt, Surinam: CO_2 fluid phase saturation during ultrahigh-temperature metamorphism

Emond W. F. de Roever[1] · Simon L. Harley[2] · Jan M. Huizenga[3,4,5]

Received: 10 September 2022 / Accepted: 4 March 2023

Abstract

The Paleoproterozoic Bakhuis Granulite Belt (BGB) in Surinam, South America, shows ultrahigh-temperature metamorphism (UHTM) at temperatures of around 1000 °C which, unusually, produced peak-to-near-peak cordierite with sillimanite and, in some cases, Al-rich orthopyroxene on a regional scale. Mg-rich cordierite (Mg/(Mg + Fe) = 0.88) in a sillimanite-bearing metapelitic granulite has a maximum birefringence of second-order blue (ca. 0.020) indicative of a considerable amount of CO_2 (> 2 wt%) within its structural channels. SIMS microanalysis confirms the presence of 2.57 ± 0.19 wt% CO_2, the highest CO_2 concentration found in natural cordierite. This high CO_2 content has enabled the stability of cordierite to extend into UHT conditions at high pressures and very low to negligible H_2O activity. Based on a modified calibration of the H_2O–CO_2 incorporation model of Harley et al. (J Metamorph Geol 20:71–86, 2002), this cordierite occupies a stability field that extends from 8.8 ± 0.6 kbar at 750 °C to 11.3 ± 0.65 kbar at 1050 °C. Volatile-saturated cordierite with 2.57 wt% CO_2 and negligible H_2O (0.04 wt%) indicates fluid-present carbonic conditions with a CO_2 activity near 1.0 at peak or near-peak pressures of 10.5–11.3 kbar under UHT temperatures of 950–1050 °C. The measured H_2O content of the cordierite in the metapelite is far too low to be consistent with partial melting at 1000–1050 °C, implying either that nearly all of any H_2O originally in this cordierite under UHT conditions was lost during post-peak cooling or that the cordierite was formed after migmatization. The high level of CO_2 required to ensure fluid saturation of the c. 11 kbar UHT cordierite is proposed to have been derived from an external, possibly mantle, source.

Keywords Ultrahigh-temperature metamorphism · Bakhuis Granulite Belt · Cordierite · CO_2 · SIMS

Introduction

Ultrahigh-temperature metamorphism (UHTM), at temperatures above 900 °C, has been described from more than 70 occurrences worldwide (Harley 2020). Characteristic UHTM mineral associations include sapphirine + quartz and Al-rich orthopyroxene + sillimanite (Harley 2020), which occur mainly in metapelitic rocks. These associations replace lower grade and/or lower pressure assemblages involving cordierite. Where cordierite occurs in UHT metapelites, it is generally interpreted to be the result of retrograde metamorphism as it typically occurs in coronas and symplectitic intergrowths around UHT minerals (e.g., Harley 1998; Kelsey and Hand 2015).

The association cordierite + sillimanite ± orthopyroxene is common in migmatitic metapelites in the Bakhuis Granulite Belt (BGB) in Surinam, South America. Feldspar thermometry on feldspar in leucosomes within such migmatitic

Communicated by Timothy L. Grove.

✉ Emond W. F. de Roever
ederoever@ziggo.nl

[1] Geology and Geochemistry Cluster, Department of Earth Sciences, VU Amsterdam, De Boelelaan 1085, 1081 HV Amsterdam, The Netherlands

[2] School of Geosciences, University of Edinburgh, James Hutton Road, Edinburgh EH9 3FE, UK

[3] Faculty of Environmental Sciences and Natural Resource Management, Norwegian University of Life Sciences, P.O. Box 5003, NO-1432 Ås, Norway

[4] Economic Geology Research Institute (EGRU), College of Science and Engineering, James Cook University, Townsville, QLD 4811, Australia

[5] Department of Geology, University of Johannesburg, Auckland Park, P. O. Box 524, Johannesburg 2006, South Africa

Published online: 03 April 2023

gneisses shows that almost the entire BGB experienced partial melting at ultrahigh-metamorphic temperatures ranging between ~ 900 and 1050 °C (Nanne et al. 2020), implying that the cordierite formed as a primary mineral during UHT metamorphism. The BGB cordierite has an elevated birefringence, indicative of a high CO_2 content (Armbruster et al. 1982) that is critical for the occurrence of primary UHTM cordierite (Nanne et al. 2020; Harley and Thompson 2004). Harley and Thompson (2004) described the behavior of cordierite and its channel volatiles CO_2 and H_2O during experimental melting, with CO_2 markedly partitioning into cordierite in the presence of a melt phase. The aim of this study is to describe the high CO_2 primary cordierite of the BGB, quantify the CO_2 contents in cordierite using different methods, and describe the tectono-metamorphic conditions that can explain its formation.

Geological setting of the Bakhuis Granulite Belt (BGB)

The BGB is situated in the centre of the Guiana Shield (the northern part of the Amazonian Craton) in the northeastern part of South America (Fig. 1) (see Nanne et al. 2020, and Beunk et al. 2021, for more details). The Guiana Shield consists mainly of Paleoproterozoic rocks, with two Archean terrains. A tonalite–greenstone coastal belt some 1500 km in length, and with an age of 2.26–2.08 Ga (Delor et al. 2003), dominates the northeastern side of the Guiana Shield. The BGB (Fig. 2), 30–40 km wide and > 100 km long, transects the greenstone belt in its centre, dividing it into two parts. The greenstone belt is considered to represent an island arc system that developed during southward subduction of the West African Craton beneath the Amazonian Craton (Delor et al. 2003). Shortly prior to its collision with the Amazonian Craton at 2.11–2.08 Ga (Delor et al. 2003), subduction of the West African plate brought the c. 100 km long Bakhuis Belt to considerable depths beneath the greenstone belt (Klaver et al. 2015; De Roever et al. 2019; Beunk et al. 2021) where it was subjected to ultrahigh-temperature metamorphism. Delor et al. (2003) proposed asthenospheric upwelling along the discontinuity in the centre of the greenstone belt—where the BGB is located—as the heat source for the metamorphism. Klaver et al. (2015) modified this hypothesis to a model of focused mantle upwelling along a major tear in the subducted West African slab as the cause for UHT metamorphism prior to or during collision. Alternatively, Beunk et al. (2021) proposed asthenospheric upwelling following slab break-off as the heat source. Extensive mafic magmatism of the same age as the UHT metamorphism has not been found

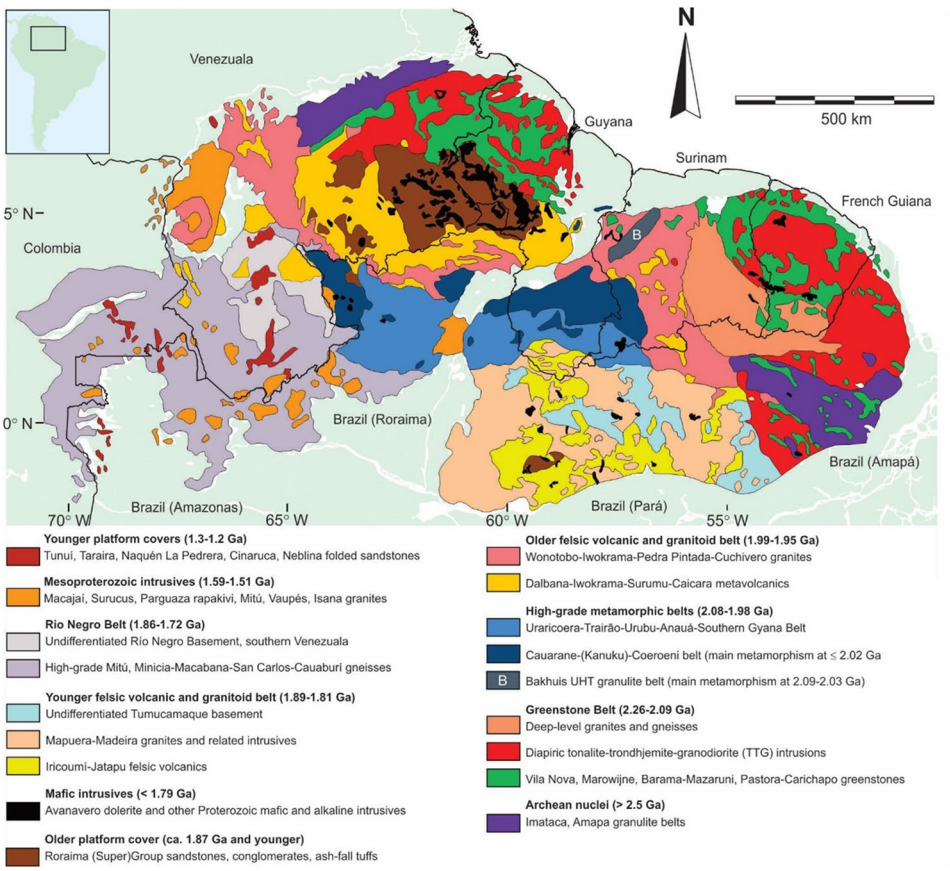

Fig. 1 Simplified geology of the northern part of the Guiana Shield (modified from Kroonenberg et al. 2016). B marks the location of the Bakhuis Granulite Belt

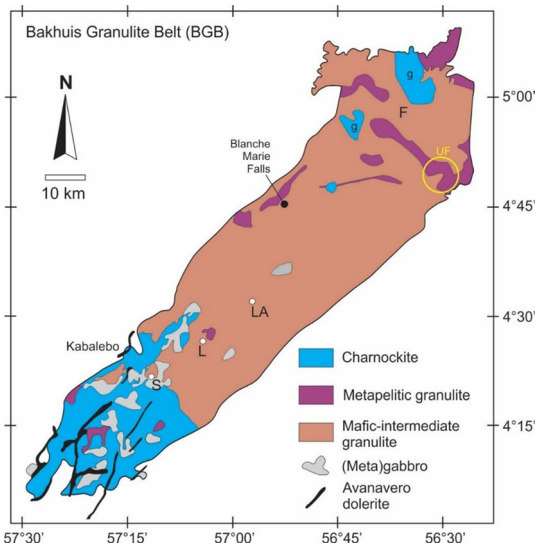

Fig. 2 Simplified geology of the Bakhuis Granulite Belt (modified after Klaver et al. 2015). *F* Fallawatra River, *UF* Upper Fallawatra area (yellow circle), *L* LJ2 and LK4 drill holes in K3 copper deposit area, *S* location of 71Sur210, *LA* drill-hole LA156, *g* biotite granite with rare orthopyroxene (instead of charnockite)

(Klaver et al. 2016). Decimetre-to-metre wide high-grade metadolerite dykes occur in the NE, centre and SW of the BGB. They were formed and subsequently deformed during UHTM (de Roever et al. 2019, 2022). They have an MgO-rich composition, with up to 15% MgO, and in part elevated Ni and Cr. They form clear evidence for mafic magmatism co-eval with UHTM, but they are too small to represent the UHTM heat source.

The UHT metamorphism of the BGB was initially dated at 2.072–2.055 Ga by Pb evaporation dating of single zircon grains (De Roever et al. 2003). Additional SHRIMP dating of zircon and monazite showed that the UHT metamorphism lasted from around 2.09–2.03 Ga. The thermal peak occurred at or shortly before 2.09 Ga, as indicated by zircon crystallisation without associated monazite at 2.088 Ga, and later crystallisation of both zircon and monazite (De Roever et al. 2019, 2022). The 2.09 Ga age overlaps with the timespan of collision of the two Cratons (2.11–2.08 Ga).

Bakhuis Granulite Belt metamorphic features

The BGB consists mainly of mafic and intermediate granulites (De Roever et al. 2003), which are characterised by regular and ubiquitous compositional banding at centimetre-to-metre scales, indicative of a predominantly supracrustal protolith, as supported by intercalations of metapelitic granulite, Ca-silicate granulite and quartzite. Mafic granulites are considered to be of volcanic origin, whereas intermediate granulites chemically resemble greywackes and intermediate volcanics (Vos 2016). The metapelitic granulites are migmatitic, with mm- to cm-wide leucosomes commonly accompanied by thicker, cm- to dm-wide leucosome layers and veins. All rock types preserve granulite–facies mineral associations. The mafic granulites consist mainly of orthopyroxene, clinopyroxene, hornblende and plagioclase. Melanocratic intermediate granulites consist of the same association together with quartz and antiperthitic plagioclase. Metapelites in most areas in the BGB consist of cordierite + sillimanite + mesoperthite or antiperthite + quartz, locally with coarse orthopyroxene. Garnet presents in some metapelites as fine-grained euhedral crystals or larger poikiloblasts formed at the expense of orthopyroxene and hence is not reflective of peak P–T conditions. Magnetite and titanohematite (with 10–15% TiO_2 besides Fe oxide) are common accessories, indicative of a considerably high oxidation state during UHTM (Nanne et al. 2020).

UHT metamorphism of the BGB is constrained by a limited number of mineral associations and mineral compositional indicators. A relatively small (50 km^2) metapelite area in the northeast of the BGB (Fig. 2), the Upper Fallawatra (UF) area, preserves the association Al-rich orthopyroxene (8–10.5 wt% Al_2O_3) + sillimanite + quartz, and locally sapphirine ± quartz (de Roever et al. 2003), both characteristic of UHT metamorphism (Harley 1998). However, the cordierite-bearing metapelites elsewhere in the BGB lack these characteristic associations and might not have formed at ultrahigh temperature. Therefore, ternary feldspar thermometry of mesoperthite and antiperthite was carried out on samples throughout the BGB. Feldspar thermometry was chosen, because it has been used in many UHTM studies (Nanne et al. 2020) and because pseudosections cannot be adequately calculated for CO_2-bearing cordierite. The study indicated peak temperatures of 900–1050 °C (Nanne et al. 2020), with T > 1020 °C in the southwest, and in the Upper Fallawatra area in the northeast (Fig. 3). Based on the feldspar thermometry results, Nanne et al. (2020) concluded that most of the Bakhuis Granulite Belt experienced UHT metamorphism and hence that the cordierite + sillimanite + mesoperthite/antiperthite + quartz association was formed at UHT conditions. This is consistent with the high Al_2O_3 contents (up to 9 wt%) of rare orthopyroxene associated with cordierite.

Pressure conditions during UHTM in the BGB are difficult to determine, in particular due to the rarity of garnet coexisting with high-Al orthopyroxene. This scarcity is the result of the considerably high oxidation state of the metapelites during UHTM, as demonstrated in Appendix 1. Phase diagrams (pseudosections) calculated in NCKFMASHTO at Fe^{3+}/Fe^{T} of > 0.57, values consistent with wet chemical analyses and the stability of magnetite and titanohematite, indicate that garnet is absent from these oxidised metapelites during UHTM at pressures less than 8.8–10.8 kbar, for temperatures of 1000–1050 °C. In the cordierite-free Upper

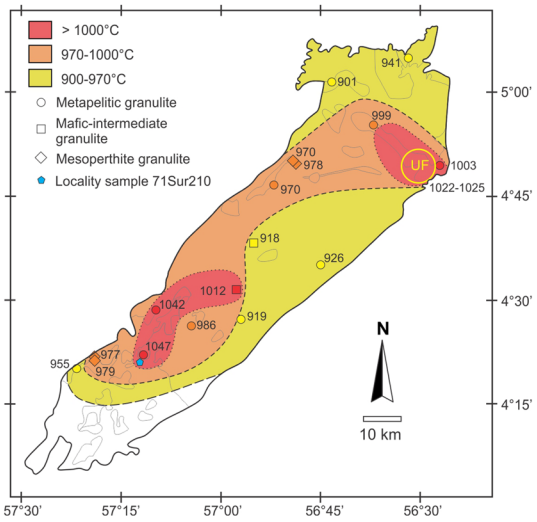

Fig. 3 Schematic map of the Bakhuis Granulite Belt with feldspar thermometry temperatures (in °C; modified from Nanne et al. 2020). For samples from the same location the highest temperature is displayed. The yellow circle in the northeast marks the Upper Fallawatra occurrence with its estimated feldspar temperature. The dashed and dotted lines mark interpreted isotherms. The site of the studied sample 71Sur210 is located at the > 1000 °C isotherm

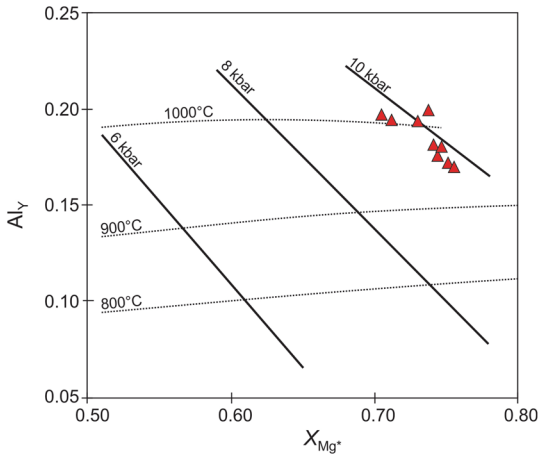

Fig. 4 Diagram from Tateishi et al. (2004), with isobars and isotherms after Hensen and Harley (1990), showing orthopyroxene composition in relation to pressure and temperature, for Opx core compositions with high Al_2O_3 (~10 wt%; triangles) from the Upper Fallawatra area, corrected for Fe^{3+}. $Al_Y = Al(VI)$; $X_{Mg^*} = Mg/(Mg + Fe^{2+})$. After Nanne et al. (2020)

Fallawatra area, only one metapelite sample was found with garnet and orthopyroxene potentially coexisting at or near-peak P–T conditions, and in that example, garnet is present apparently included in a large orthopyroxene grain that is rimmed by coronal garnet. Using the temperature provided by feldspar thermometry, a pressure of 9 kbar was calculated using the calibration of Harley and Green (1982) for this occurrence (Nanne et al. 2020). In light of the phase diagram calculations performed on the UF metapelites (Appendix 1), this garnet is considered to represent post-peak garnet formed on cooling as part of the coronal rim, consistent with the lack of Ti-oxide exsolution in both the inclusion and coronal garnet (see Appendix 2). In view of the lack of demonstrably co-eval garnet, Nanne et al. (2020) estimated pressure on the basis of Mg–Al covariation in orthopyroxene coexisting with sillimanite + quartz (thereby containing the maximum level of Al_2O_3 possible at the P–T of formation), following the semi-quantitative methodology of Tateishi et al. (2004; based on Hensen and Harley (1990). Pressures of 9.5–10 kbar at temperatures of 940–1020 °C were estimated for the 10 wt% Al_2O_3 orthopyroxene preserved in the UF metapelitic granulites (Nanne et al. 2020; Fig. 4). Calculated phase diagrams for UF metapelites (Appendix 1) indicate temperatures of > 1000 °C for the presence of orthopyroxene with such Al_2O_3 content, which corresponds to 20–22 mol% Tschermaks component. The calculated phase diagrams also are in agreement with the high feldspar temperatures found for metapelites of the UF area (1022–1025 °C; Fig. 3). Ternary feldspar with the composition $Or_{12}Ab_{60}An_{28}$ is calculated to be present at 8.5–9.5 kbar and T > 1035 °C with Opx + Sill + Qz + Ti-Hem + Mt in UF sample SB24a (Appendix 1) (mineral abbreviations follow Whitney and Evans 2010).

Recently, garnet in some garnet- and garnet–sillimanite–granulites in the northeast of the BGB, near the UF area, was found to contain oriented TiO_2 needles (see Appendix 2), which most likely represent exsolution from precursor UHT garnet (see Ague 2012; Gou et al. 2014; Keller and Ague 2019). For a garnet-bearing metapelitic granulite occurring NE of the UF area (Fig. 3), a feldspar temperature of 1003 °C was determined on mesoperthite (Nanne et al. 2020). Using the Ca-in-garnet barometer of Wu (2019) and the temperature mentioned, pressures of 10.7–11.7 kbar were calculated for the garnet, with an average value of 11.1 ± 0.5 kbar.

In summary, whilst peak temperatures for UHT metamorphism of the BGB in excess of 1000 °C are reasonably well established from feldspar thermometry and Al_2O_3 in orthopyroxene constraints, the pressures at peak-T (1020–1050 °C) across the BGB are loosely constrained to be of the order of 9–11 kbar on the basis of pressure estimates for the UF area in the northeast of the BGB and the nearby UHT garnet granulite noted above, and the restriction of garnet to high pressures in the oxidised bulk rock compositions (Appendix 1).

The UHT metamorphism of the BGB granulites is overprinted by retrograde metamorphism and considerable deformation. Mylonitisation during the Nickerie Tectonometamorphic Event at 1.2 Ga (see Beunk et al. 2021) was accompanied by low-grade metamorphism.

In the BGB, fluid inclusions (FI) are fairly common in quartz (and feldspar) in leucosomes in metapelite and in intermediate granulites. Most fluid inclusions have a marked relief under the microscope, indicative of dominant CO_2. The FI of 11 granulite samples were used for a C^{13}/C^{12} analysis (Donker 2021). One of the samples was used as a reference sample in the C- and O-isotope study of Luciani et al. (2022). They determined a $\delta^{13}C$ value of -4.5 ± 0.8 for CO_2 in fluid inclusions in quartz in granulite from Blanche Marie Falls, in the core of the BGB (Fig. 2). They found only CO_2, without any water (and without N_2), by Raman spectroscopy. Another study also showed FI with CO_2 without visible water, in quartz in the leucosome of an intermediate granulite from the centre of the BGB (location LA in Fig. 2), accompanied by some brine fluid inclusions (for details and images, see Touret et al. 2016). Fluid inclusions in cordierite were rarely found. Cordierite in a quartzite from the K3 area in the southwest of the BGB showed fluid inclusions with the marked relief indicative of dominant CO_2.

Cordierite-bearing metapelites and quartzites

Metapelitic gneisses outside the Upper Fallawatra area typically contain coarse cordierite and sillimanite, locally accompanied by coarse aluminous orthopyroxene (Fig. 5). The relatively coarse grain-size of the Crd, Sil and Opx, mainly in the mm-range, but in cases up to 1–2 cm, indicates that they form part of the peak metamorphic assemblage. The metapelites show widespread and considerable recrystallization due to retrograde metamorphism and younger deformation phases, including locally strong mylonitization. Most cordierite recrystallized partially, e.g., along its rims, into fine-grained sillimanite, orthopyroxene, biotite and kyanite or andalusite. More advanced recrystallization produced fine-grained aggregates of these minerals, with or without Crd relics.

In a few samples from the southwestern part of the BGB, cordierite occurs in the form of symplectitic intergrowths with sapphirine around or next to coarse sillimanite (De Roever et al. 2003). These intergrowths might have formed from a former peak metamorphic mineral, possibly orthopyroxene. A few orthopyroxene grains were found in two samples with intergrowths, but not near or adjacent to them. The intergrowths might also have formed at the expense of sillimanite (compare Harley 2020).

In the K3 area in the southwest of the BGB, two samples of cordierite quartzite have been found (Fig. 5). Both samples contain approx. 20 vol% cordierite and rare garnet and orthopyroxene. One sample contains ~ 1–2 vol% plagioclase, and the other one around 10%.

Analytical methods

Electron probe microanalysis

The cordierite composition was obtained with wavelength-dispersive spectrometry on the JEOL-JXA-8800 M

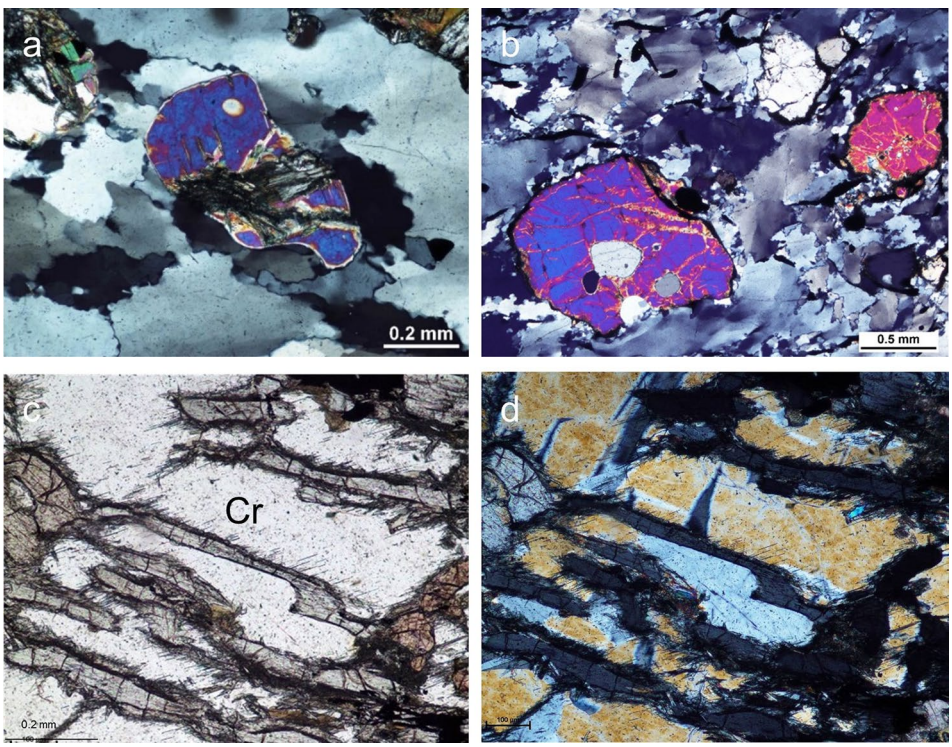

Fig. 5 **a** Blue birefringent cordierite in leucosome quartz, sample LK4-47 m, crossed polarized light (XPL). **b** Blue and red birefringent cordierite grains in quartzite, RG1457, XPL. **c** Coarse intergrowth of Crd with Opx, drill-core LJ2-25.5 m. Plane polarized light (PPL). **d** Same image, XPL

microprobe at Vrije Universiteit Amsterdam, using a 15 kV accelerating voltage and a 25 nA beam current. Counting times were typically 25 s on peaks and 12.5 s on background for major elements. For minor elements, it was set to 36 s on peaks and 18 s on background. Natural mineral standards and a ZAF matrix correction routine were used (Armstrong 1988). A cation-based mineral formula was used, assuming all iron to be ferrous.

SIMS analysis

The analytical procedures and conditions for SIMS analysis of natural cordierite have been outlined in Harley et al. (2002). Cordierite in a polished, gold-coated thin section was analysed in situ with a Cameca IMS-4f ion probe (School of Geosciences, University of Edinburgh) using negative secondary ions (^{1}H, ^{12}C and ^{28}Si) measured at an energy offset of 60 V. The primary ion beam is O-, sourced from a duoplasmatron and accelerated through 10 kV at a beam current of 7 or 8 nA. The secondary ion beam is 4.5 kV. Each analysis involves a 3-min burn-in time followed by 30 cycles of 5 s counts for each isotope, producing a roughly 30 µm diameter and 3 µm deep sputtered pit. The mean of the isotope ratios of the last 10 cycles is taken as the final result, thereby avoiding surface contamination. Typically, 6–12 spot analyses of cordierite are obtained for a sample. Analyses were obtained as isotopic ratios of $^{1}H/^{28}Si$ and $^{12}C/^{28}Si$ and then converted to wt% H_2O or CO_2 by comparison with the calibration lines from standards analysed in the same session. Two natural cordierite grains with H_2O and CO_2 contents measured by independent methods (H-manometry, coulometric titration, stepped-heating mass spectrometry) were used as primary standards (AMNH and 8/90). Standard AMNH is Mg rich ($X_{Mg} = 0.87$, where X_{Mg} denotes the molar Mg/(Mg + Fe) ratio), and has H_2O and CO_2 contents of 1.56 ± 0.08 wt%, and 0.70 ± 0.05 wt%, respectively. Standard 8/90 (referred to as 81/90 in Harley et al. 2002) has an intermediate Mg content ($X_{Mg} = 0.66$) and H_2O and CO_2 contents of 0.80 ± 0.06 wt%, and 1.30 ± 0.06 wt% respectively. Two further natural cordierites with low (0.47 wt%, 49528) and high (1.9 wt%, 15/90) CO_2 contents, respectively, analysed along with the two primary standards in several earlier and separate sessions, were used to constrain the curvature of the polynomial fit required to convert C/Si to wt% CO_2, described in detail in Appendix 3. The high CO_2 sample 15/90 was provided to the Edinburgh IMF by Prof. V. Schenk in 1990. It was analysed using stepped-heating mass spectrometry at RHUL following the procedures of Fitzsimons and Mattey (1995) to yield a bulk CO_2 content of 1.88 ± 0.09 wt%. Analysis of this sample in several SIMS sessions along with AMNH and 8/90 produced consistent calibration curves. SIMS analysis errors based on these calibration curves are typically ± 12% relative for H_2O and ± 8% relative for CO_2.

Raman microspectroscopy

Raman spectra were acquired from cordierite in polished thin sections with a Renishaw InVia Reflex Raman Microscope at the Vrije Universiteit Amsterdam in backscatter mode, using an 80 mW, 532 nm laser and an 1800–1/mm grating. The instrument includes a Leica polarized light microscope. An internal silicon standard (521 cm^{-1}) was used to verify the spectral calibration of the system. Lorentzian peak fit was applied to determine the peak centre and peak height of the cordierite spectrum. Selected grains were oriented properly to acquire a high CO_2 signal.

Birefringence

The precise determination of the cordierite birefringence proved to be difficult. Most samples contain rather small amounts of cordierite that are too small for separation. Therefore, the birefringence was estimated in two ways. The maximum interference colour in thin sections of standard thickness (~ 30 µm) was used as a first approximation. For a more precise result, a Berek compensator was used to determine the retardation (see, e.g., Muir 1967) of the cordierite grain with the maximum interference colour in the thin section. Its orientation should provide a (nearly) centred flash figure. The retardation for quartz was determined by establishing the maximum interference; the crystallographic orientation of quartz was checked by the presence of a flash interference figure. Based on the quartz birefringence (0.009), the cordierite birefringence could then be calculated. The calculation represents only an approximation as both the cordierite and quartz grains may not be in optimal orientation. In many samples, this method could not be used because of marked quartz deformation (a common phenomenon in the BGB).

Results

Electron microprobe analysis

Cordierite is Mg-rich ($X_{Mg} = 0.83$–0.92). Alkalies (Na_2O) make up less than 0.05 wt% in most analyses, and CaO and K_2O are less than 0.01 wt% (Table 1). Low total sums of 94.1–97.3 wt% are consistent with the presence of appreciable H_2O and/or CO_2. Cordierite in cordierite-sapphirine intergrowths is slightly higher in X_{Mg}.

Table 1 Microprobe analyses of BGB cordierite

	FN72A	FN86	FN27	FN05	SA776	LJ2-30	71Sur210	RG1054	RG1508
SiO_2	48.68	49.30	48.49	48.90	49.45	48.51	47.96	48.40	48.38
Al_2O_3	32.41	32.54	32.39	32.68	33.80	32.63	31.82	33.10	32.71
FeO*	3.58	3.13	2.69	2.53	2.56	2.36	2.22	2.20	1.81
MnO	0.32	0.39	0.18	0.18	0.10	0.19	0.15	0.22	0.19
MgO	10.67	10.77	11.15	11.47	11.40	11.43	11.92	11.60	11.89
Na_2O	0.03	0.02	0.02	0.03	0.00	0.01	0.01	0.08	0.01
Total	95.70	96.16	94.97	95.79	97.30	95.15	94.08	95.60	94.99
Si	5.05	5.08	5.04	5.03	5.01	5.02	5.01	4.99	5.00
Al	3.96	3.95	3.97	3.96	4.04	3.98	3.93	4.02	3.99
Fe	0.31	0.27	0.23	0.22	0.22	0.20	0.19	0.19	0.16
Mn	0.03	0.03	0.02	0.02	0.01	0.01	0.01	0.02	0.02
Mg	1.65	1.66	1.73	1.76	1.72	1.77	1.85	1.77	1.83
Na	0.01	0.00	0.00	0.01	0.00	0.00	0.00	0.02	0.00
Normalised to 11 cations									
X_{Mg}	0.84	0.86	0.88	0.89	0.89	0.90	0.91	0.90	0.92

Cordierite in RG1508 and RG1054 occurs in part in Crd–Spr intergrowths. Most analysed cordierites have a blue maximum birefringence, except FN27 and FN05 cordierite

FeO* denotes total iron as FeO

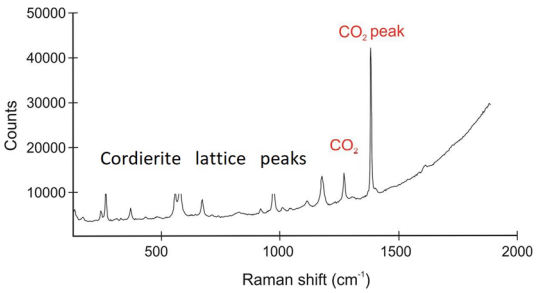

Fig. 6 Raman spectrum of blue birefringent cordierite from sample 71Sur210. Vertical scale in arbitrary units; horizontal scale shows the Raman shift in cm^{-1}. The grain selected was oriented optimally to acquire the highest CO_2 signal. Note the height of the main CO_2 peak compared to the Crd lattice peaks. After Nanne et al. (2020)

Raman microspectroscopy

Raman microscopy was used as a first step to establish the identity of the volatiles, H_2O and CO_2, present in the channels in the cordierite. The Raman spectrum of a blue birefringent cordierite grain in sample 71Sur210 shows a very strong CO_2 band at 1380 cm^{-1} and less strong bands of cordierite (Fig. 6). H_2O bands, which would occur near 3600 cm^{-1}, were absent in this sample and very weak in another cordierite (sample SA776), which in addition showed a very weak band for N_2. Granulite–facies cordierite from elsewhere may contain up to 4000 ppm N_2 (Bebout et al. 2016).

Raman microscopy may be used to estimate the cordierite CO_2 content from the linear correlation between CO_2 wt% and the intensity ratios of the CO_2 mode at 1380 cm^{-1} and the cordierite lattice vibration modes at 973 cm^{-1} and 1185 cm^{-1} (Kaindl et al. 2006). This method would indicate the presence of 2.5–3 wt% CO_2 in the 71Sur210 cordierite, but considerable extrapolation was required from standards that only contain up to 1.5 wt% CO_2.

Birefringence

A striking feature of many cordierite grains is their elevated birefringence, with maximal interference colours ranging up to first-order orange and red and second-order blue (Fig. 5) in standard thin sections. Whilst cordierite birefringence increases markedly with Fe content (e.g., Deer et al. 1997), the BGB cordierite is Mg-rich (X_{Mg} 0.83–0.92), and for such compositions, the birefringence depends strongly on CO_2 content. This is illustrated in the cordierite volatile component diagram of Armbruster et al. (1982; Fig. 7), in which the birefringence (red lines) for the X_{Mg} 0.85 Valjok cordierite equilibrated with CO_2, H_2O, and H_2O–CO_2 fluids is seen to increase principally with increasing CO_2 in the cordierite.

The birefringence of BGB cordierite was first estimated assuming a standard thin section thickness of 30 µm. On this basis, the maximum interference colour, second-order blue, would correspond to a birefringence of approximately 0.021 ± 0.001 (e.g., Nesse 2000). The cordierite birefringence was also analysed with a Berek compensator. For metapelite samples 71Sur210 (in the southwest of the BGB) and SA776 (in the northeast), a cordierite birefringence of 0.020 was determined. For cordierite in metapelite samples FN04 (lower Fallawatra area) and LK4-47 m,

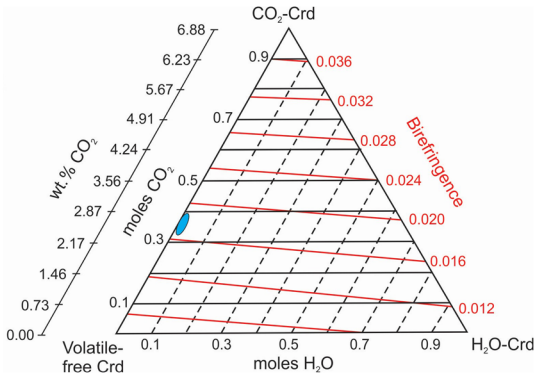

Fig. 7 Influence of channel filling by CO_2 and H_2O on cordierite birefringence, based on experiments with Valjok Crd (X_{Mg} 0.85), modified from Armbruster et al. (1982). The corners of the triangle represent Gas-free Crd, pure CO_2-Crd with one mole CO_2 (6.88 wt%), and pure H_2O-Crd with one mole H_2O (2.93 wt%). Diagram data are extrapolated above 0.43 mol CO_2 and 0.85 mol H_2O. Blue marked area: SIMS analysis of 71Sur210 cordierite

and in quartzite RG1459 (the latter two samples are from the K3 area in the southwest), a birefringence of 0.021 was determined.

SIMS analysis

Sample 71Sur210, a mylonitic pelitic granulite from the SW of the BGB, with cordierite with a maximum interference colour of second-order blue and a birefringence of 0.020 (for additional details, see Appendix 4), was selected for analysis on the Cameca Ims-4f SIMS instrument at the School of GeoSciences, Edinburgh, following the approach of Thompson et al. (2001) and Harley et al. (2002). Sixteen SIMS analyses were carried out in situ on 12 grains, with 3 grains having more than one analysis. Following analysis the SIMS spots were examined under reflected and transmitted light to detect whether any cracks or areas of near-rim alteration

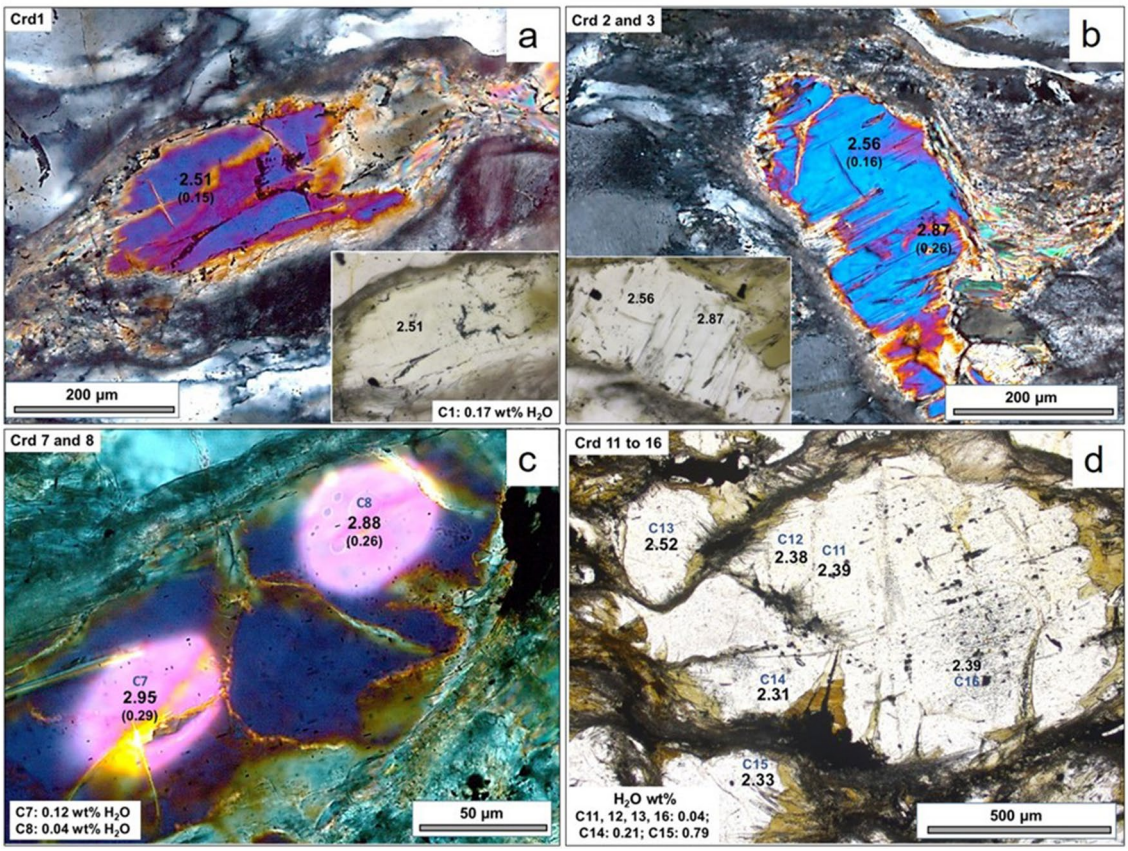

Fig. 8 Photomicrographs of selected analysed cordierite grains in sample 71Sur210. Numbers on each are the measured CO_2 contents in wt%, with associated uncertainties in brackets shown in some cases. Labels C7, C8, C11, etc. refer to the analysis point identifiers as listed in Table 2 and shown in Fig. 9. H_2O wt% values for each analysis in (**a**), (**c**) and (**d**) are shown in the inset boxes. Micrographs (**a**), (**b**) and (**c**) are under crossed polars. **a** and **b** show the strong mylonitic fabric that wraps the cordierite blasts, the late biotite beards and alterations on cordierite, and highlight the second-order pink to blue birefringence of the CO_2-rich cordierite. Plane polarized light (PPL) images of the same grains are added in the insets to these micrographs. **c** Two SIMS analysis sites. The analysis spots are ca. 20–25 µm diameter, but the pre-analysis rastering leaves a sputtered surface c 50 µm across. **d** PPL image of a large cordierite blast, analyses C11, C12, C14 and C16, and two adjacent grains (C13 and C15). Note the homogeneity of the large cordierite in terms of CO_2 content. Analyses C14 and C15, both near biotite alteration rinds, have elevated H_2O compared with the other analyses. See text for discussion

had been incorporated into the analysis, and to document the interference colour of the analysis region (Fig. 8).

Twelve of the 16 analyses, including two from grain 2 (C2 and C3) and three from grain 9 (C11, C12 and C16) form a population characterised by very low H_2O contents (0.037 ± 0.01 wt%). This analytical population, all obtained from clean analysis sites, ranges from 2.88 to 2.39 wt% CO_2, with an average of 2.57 ± 0.19 wt% CO_2 (Fig. 9). Combining this CO_2 content with the very low H_2O (c. 0.04 wt%) yields average cordierite molar volatile parameters of $n(_{H2O}) = 0.012 \pm 0.003$ and $m(_{CO2}) = 0.351 \pm 0.023$. Based on this, the measured cordierite channel volatile composition, X_{CO2} (Crd), is 0.996 ± 0.002.

Four analyses (one each from grains 1, 6, 11, and 12) were located on sites containing one or more cracks or potentially incorporating altered subareas. Whilst the CO_2 contents obtained for these points (2.31–2.95 wt%) were consistent with those from the cleaner or not evidently contaminated sites (Fig. 8) as their elevated H_2O contents (0.12–0.79 wt% H_2O) may reflect contamination, they have been excluded from calculation of the average CO_2 and H_2O contents for the population. One analysis, C15 from grain 12, is measured to contain 0.79 wt% H_2O, far higher than all other analyses. As noted above, the preferred interpretation of the elevated H_2O is contamination arising from the incorporation of thin biotite flakes or fine clays along cracks present at the analysis site. However, if the elevated H_2O is real and within the cordierite itself, then this may imply that all the other cordierite analysis sites have been affected by H_2O loss. This possibility is considered in the Discussion.

In summary, SIMS analysis indicates that the preserved cordierite contains 2.57 ± 0.19 wt% CO_2 and 0.04 ± 0.01 wt% H_2O. With its measured channel X_{CO2} of 0.996, it is the most pure CO_2-cordierite ever recorded.

Discussion

The c. 2.6 wt% CO_2 found by SIMS analysis for BGB cordierite is the highest level found in natural cordierite. Prior to this work, the highest level was c. 2.2 wt% CO_2 in cordierite from Valjok in the northernmost part of the Granulite Belt of Lapland in Norway (Armbruster et al. 1982). The Valjok cordierite contained 0.3 wt% H_2O, giving a X_{CO2} of 0.75 and suggesting a coexisting fluid of $X_{CO2} > 0.95$ (Armbruster et al. 1982). Based on the majority of SIMS analyses, the BGB cordierite is almost H_2O-free (0.037 wt% H_2O), has a channel X_{CO2} of 0.996, and hence implies equilibration with a coexisting fluid of $X_{CO2} > 0.996$ (Harley et al. 2002): essentially pure CO_2.

SIMS analysis of the BGB cordierite indicates that birefringence is a reasonable indicator of CO_2 contents in cordierite but must be applied with some caution if quantitative results are required. The SIMS results when plotted on the diagram of Armbruster et al. (1982; Fig. 7) would indicate a birefringence of 0.018 ± 0.001, corresponding to second-order magenta rather than the blue maximum interference colours observed (e.g., grain 2).

Blue birefringent cordierite with > 2 wt% CO_2, as found in the 71Sur210 sample, is not rare in the BGB, but has been found in 22 out of 66 metapelite samples from several localities throughout the belt (Fig. 10). However, half of the Bakhuis cordierites show a considerably lower maximum birefringence, yellow and orange, suggesting a lower CO_2 level in the 1.5–2 wt% range, the reasons for which are unknown as these cordierites have not as yet been investigated.

P–T conditions for CO_2-rich cordierite from the BGB

Iso-CO_2 lines for X_{Mg} 0.88 cordierite with 2.57 ± 0.17 wt% CO_2 have been calculated based on the P–T-dependent CO_2 incorporation model of Harley et al (2002). As has been the case with previous work (Harley 2008), the preliminary ΔV_s, ΔH_r and ΔS_r values reported in Harley et al (2002) have been adjusted to better fit the Thompson et al. (2001) experimental data along with their further unpublished experimental data at 800–1000 °C and 3–7 kbar, and be in reasonable accord with experimental results from other studies (Armbruster and Bloss 1980; Johannes and Schreyer 1981; Kurepin 1985; LeBreton and Schreyer 1993). The revised best-fit parameters used

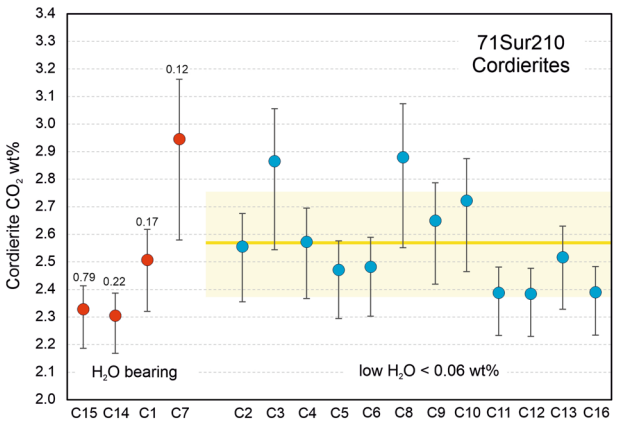

Fig. 9 SIMS CO_2 results for 71Sur210 cordierites. Labels on the horizontal axis are the analysis numbers. Those analyses with $H_2O > 0.1$ wt% are distinguished by the filled red circle symbol, and those with $H_2O < 0.06$ wt% by the blue filled circle symbols. Error bars are 2 sigma uncertainties associated with the polynomial SIMS calibration used to reduce the raw C/Si data. Decimal numbers attached to the four H_2O-bearing analyses are the measured H_2O contents. The bright yellow line is the average CO_2 content calculated from the 12 low-H_2O cordierite analyses (2.57 wt%) and the paler yellow area the associated uncertainty (±0.19 wt%)

are $\Delta V_s = 2.112$ Jmol^{-1}, $\Delta H_r = -16.56$ kJmol^{-1} and $\Delta S_r = -102.43$ Jmol^{-1} K^{-1}.

The resultant isolines for the Bakhuis cordierite constrain the yellow shaded field (Fig. 11) that occurs from 9.2 ± 0.6 kbar at 800 °C to 10.9 ± 0.65 kbar at 1000 °C and 11.7 ± 0.7 kbar at 1100 °C. Volatile-saturated cordierite with 2.57 wt% CO_2 and negligible H_2O (i.e., $a_{CO2} = 1$) requires pressures of 10.5–11.3 kbar at 950–1050 °C via this model. The original Harley et al.'s (2002) model calibration applied to the same cordierite results in pressure estimates of 13.4 kbar at 1000 °C and 11.7 kbar at 900 °C, that are untenable as they exceed the experimentally constrained upper pressure limit for X_{Mg} 0.88–0.92 cordierite as constrained by Bertrand et al. (1991). It should be noted that the estimated pressures obtained through either calibration are well outside the 3–7 kbar range covered by the experiments on which the calibrations are based, and hence are less robust than pressure estimates for lower CO_2 cordierites. Nevertheless, the calculated pressures of 10.9 ± 0.7 kbar at 1000ºC obtained here are considered to be reasonable for the BGB.

The line in Fig. 11 labelled 'Kurepin Eq34' is the P–T locus of cordierite with 2.57 wt% CO_2 according to the model proposed by Kurepin (2010). Despite noting the presence of a volume term in both the Harley et al (2002) and Armbruster and Bloss (1980) experimental results for CO_2-bearing cordierite, and explaining it in terms of differential thermal expansions of CO_2-free and CO_2-rich cordierite, Kurepin (2010) did not go on to include such a term in his model. This omission results in the much lower pressures, 7.4–8.2 kbar at 900–1000 °C, estimated from his equation when applied to the Bakhuis cordierites. These pressures are significantly less than the independent pressure estimates of Nanne et al. (2020) and hence unlikely to be realistic.

The line in Fig. 11 labelled 'Bertrand et al (1991)' is the experimentally constrained estimate for pure CO_2 cordierite stability in FMASHC in the presence of Grt + Sil + Qz or Opx + Sil + Qz, applicable to cordierites with X_{Mg} similar to the Bakhuis example. The line fitted by Bertrand et al (1991) to their pure-CO_2 experiments marking the transition from the Grt + Crd + Sil + Qz assemblage to

Table 2 SIMS results on Cordierite 71Sur210

Cordierite volatile compositions							Activities (Crd)			Crd/Melt H_2O	
Analysis	H_2O	CO_2	n(H_2O)	m(CO_2)	X_{CO2}crd	m + n	a_{H2O}	a_{CO2}	a_{total}	D_w	Melt H_2O
Analyses with significant H_2O											
C15	0.792	2.330	0.264	0.317	0.546	0.581	0.082	0.862	0.943	2.15	1.70
C14	0.218	2.307	0.072	0.314	0.813	0.387	0.018	0.849	0.867	3.25	0.71
C1	0.173	2.509	0.058	0.342	0.856	0.399	0.014	0.962	0.976	3.58	0.62
C7	0.119	2.947	0.040	0.401	0.910	0.441	0.009	1.243	1.253	4.21	0.50
Average	0.109	2.561	0.036	0.349	0.920	0.385	0.010	0.998	1.008		
Main group: analyses with negligible H_2O											
C12	0.059	2.385	0.020	0.325	0.943	0.345	0.005	0.892	0.896	5.80	0.34
C13	0.047	2.517	0.015	0.343	0.957	0.358	0.004	0.967	0.971	6.49	0.30
C10	0.042	2.722	0.014	0.371	0.963	0.385	0.003	1.092	1.096	6.79	0.29
C4	0.040	2.575	0.013	0.351	0.963	0.364	0.003	1.001	1.004	6.97	0.28
C8	0.039	2.880	0.013	0.392	0.968	0.405	0.003	1.196	1.199	7.07	0.27
C6	0.037	2.483	0.012	0.338	0.965	0.351	0.003	0.947	0.950	7.21	0.27
C9	0.035	2.650	0.012	0.361	0.969	0.373	0.003	1.047	1.050	7.40	0.26
C2	0.034	2.558	0.011	0.348	0.968	0.360	0.003	0.991	0.994	7.50	0.26
C3	0.031	2.867	0.010	0.391	0.974	0.401	0.002	1.188	1.190	7.90	0.24
C11	0.031	2.389	0.010	0.325	0.970	0.336	0.002	0.894	0.896	7.92	0.24
C5	0.029	2.473	0.010	0.337	0.972	0.347	0.002	0.942	0.944	8.12	0.24
C16	0.019	2.391	0.006	0.326	0.981	0.332	0.001	0.895	0.896	9.85	0.19
Average	0.037	2.574	0.012	0.351	0.966	0.363	0.003	1.004	1.007	7.42	0.27
stdev	0.010	0.174	0.003	0.024	0.009	0.024	0.001	0.107	0.107	1.01	0.04

Volatile contents in wt% H_2O and CO_2 are converted to molar contents n(H_2O) and m(CO_2) assuming cordierite is X_{Mg} 0.88. Cordierite channel volatile composition is X_{CO2}Crd, and total volatiles summed as m + n in moles pfu. Activities of H_2O and CO_2 are calculated at 11.3 kbar and 1050 °C based on the methods of Harley et al. (2002) with the model calibration modifications noted in the text. Total fluid activity is denoted as a_{total}. Hypothetical melt H_2O contents are estimated based on the D_w expression of Harley and Carrington (2001) and Harley et al. (2002). These hypothetical melt H_2O contents are negligible for the main group of cordierite analyses (0.27 ± 0.04 wt%), and for all of the potentially contaminated analyses apart for C15, and lie far below any wt% H_2O that would allow a broadly granitic melt to be present at these P–T conditions

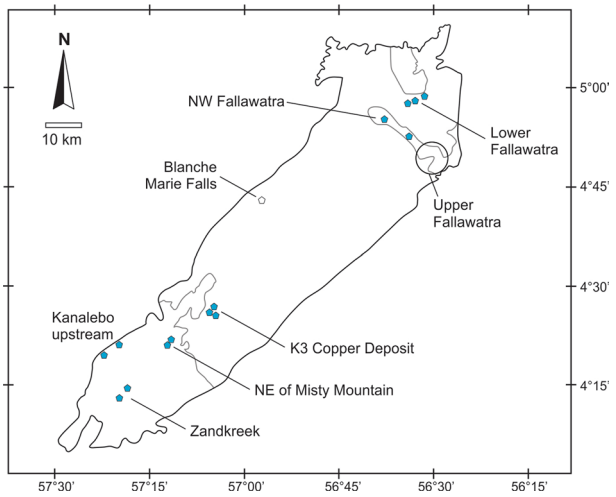

Fig. 10 Distribution of blue birefringent cordierite (blue diamonds) in metapelites in the BGB. Empty diamond at Blanche Marie Falls: metapelite with cordierite of lower maximum birefringence

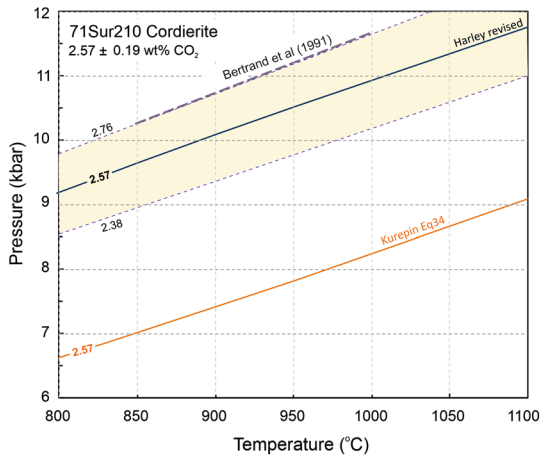

Fig. 11 Cordierite iso-CO_2 lines based on the Harley et al (2002) model, with re-fitted ΔV, ΔH, and ΔS parameters (blue lines and yellow field) and the model of Kurepin (2010) (orange line). The experimentally determined position of Grt + Opx + Sil + Crd + Qz for pure CO_2 conditions determined by Bertrand et al. (1991) is shown as the dark dashed line, which has a pressure uncertainty of ± 0.5 kbar

the Opx + Crd + Sil + Qz one is essentially parallel to the cordierite iso-CO_2 lines as modelled here based on Harley et al. (2002), and would be consistent with their experimental cordierites containing c. 2.77 wt% CO_2 (m = 0.378). The presence of Opx + Sil + Qz in the Bertrand et al. (1991) experiments at 11 kbar and 850–900 °C indicates that high-CO_2 magnesian cordierite stable at 1000 °C would be replaced by Opx + Sil + Qz on near-isobaric cooling.

Supporting P–T estimates

As described in the section "Bakhuis Granulite Belt metamorphic features", estimates of peak-T pressures for the Bakhuis metamorphic belt are in the range 9–11 kbar and mainly based on Mg–Al covariation in Opx (+ Sil) in the Upper Fallawatra area in the northeast of the belt (Nanne et al. 2020) and on the Ca-content of garnet in one sample of pelitic granulite occurring NE of the UF area, which yielded a pressure of 10.7–11.7 kbar using the barometer of Wu (2019). These estimates overlap with but also range to 2 kbar lower than those deduced from the high-CO_2 cordierites based on the modified Harley et al.'s (2002) model. The differences may reflect the combination of uncertainties in the cordierite modelling (i.e., modified Harley et al. (2002) vs. Kurepin (2010)) and those inherent in Ca-in-garnet geobarometry and semi-quantitative orthopyroxene–sillimanite–quartz thermobarometers. On the other hand, they may be real and indicative of regional variations across the extensive Bakhuis Granulite Belt. Several sites where highly birefringent cordierite is present may have differed in their peak-T pressures from those determined for the Upper Fallawatra area in the northeast of the BGB.

As noted in a previous section and detailed in Appendix 1, phase diagram calculations on 5 oxidised metapelitic granulites from the northeast and southwest of the BGB indicate stability of the garnet-absent Opx + Sil + Qz + Mt + Ti-Hem assemblage in such rocks at pressures up to 8.8–10.6 kbar at temperatures of 1000–1050 °C, in the absence of CO_2. These upper pressure limits apply for bulk rock Fe^{3+}/Fe^{T} values of c. 0.65, a conservative oxidation state which is consistent with the dominance of titanohematite along with the presence of magnetite in these rocks. The Opx + Sil + 2-Feldspars/ternary feldspar + Qz + Ti-Hem + Mt ± L assemblages preserved in the UF rocks also yield calculated temperatures of > 1000 °C based on the core Al_2O_3 contents of their orthopyroxenes.

To explore the limits on the cordierite and Opx + Sil + Qz assemblages of relevance to the present sample, phase diagram calculations have been carried out on model cordierite bulk compositions. The calculated phase diagrams have been constructed in Theriak–Domino (de Capitani and Petrakakis 2010) using Thermocalc datasets ds5.5 and ds6 (Holland and Powell 2011; White et al. 2014) (Fig. 12). These show that volatile-free cordierite with X_{Mg} of 0.88 is only stable to c. 6.5–7.2 kbar at 900–1000 °C and the Crd + Sil + Opx + Qz assemblage to only 7–7.5 kbar. Similar X_{Mg} (= 0.85) cordierite with 0.5 mol pfu of H_2O is stable to 8.0–8.5 kbar and succeeded by Crd + Opx + Sil + Qz to 9.1–9.8 kbar at 900–1000 °C. The orthopyroxene coexisting with X_{Mg} 0.88 cordierite in this assemblage has the equivalent of 10 wt% Al_2O_3 at 960–1020 °C (Fig. 12).

In Fig. 12b, the cordierite isopleth field for 2.57 ± 0.19 wt% CO_2 as calculated using the modified Harley et al.'s

(2002) cordierite model (grey field) is superimposed on a model phase diagram in FMAS for H_2O-free (i.e., dry) X_{Mg} 0.88 cordierite calculated in Theriak–Domino (de Capitani and Petrakakis 2010) using Thermocalc dataset 5.5 (Holland and Powell 2011). The phase diagram is contoured for mole proportion of MgTs in Al orthopyroxene in the assemblages that lie beyond cordierite stability. Note that volatile-free cordierite (blue field in Fig. 12a) is restricted to pressures less than c. 7.3 kbar at 1050 °C, some 4 kbar lower than the pressures deduced from the CO_2-saturation isopleths. The addition of CO_2, which is wholly incorporated into cordierite in the absence of melt, extends the stability of cordierite. Following Schreinemakers principles, the Crd-only field expands up pressure along the locus of the (Crd) line [i.e., the line between the Opx + Sil + Qz and Opx + Spr + Qz fields], so that the pseudoinvariant point involving Crd, Opx, Sil, Spr and Qz would occur at c. 12 kbar and 1150ºC, for the water-free, high-CO_2 cordierite (blue field in Fig. 12b). The likely impact of this is illustrated in Fig. 13, discussed below.

Migmatisation and the low H_2O content of BGB UHT cordierite

The BGB metapelites are migmatitic. Their partial melting occurred during the thermal peak of UHT metamorphism in view of the high temperatures found for feldspar from the leucosomes by feldspar thermometry (Fig. 3; Nanne et al. 2020), with peak temperatures of 1020–1050 °C for parts of the belt. Harley and Thompson (2004) described the behavior of cordierite and its channel volatiles CO_2 and H_2O in volatile-saturated experiments with coexisting granitic melt. CO_2 was found to partition very strongly into cordierite over melt (Dc > 10), so that CO_2-rich cordierite could occur at high P–T conditions along with melt containing low H_2O. The minimum H_2O that could be present in the melt would depend on the a_{H2O} and the position of the relevant solidus at that P–T condition. In the BGB case, the a_{H2O} calculated from the cordierite compositions at 1000–1050 °C is only 0.003. At 11.3 kbar and 1050 °C, this reduced a_{H2O} would be far too low to enable the proportion of melting evident in much of the BGB. The melt H_2O content calculated from the cordierites using the relations of Harley et al (2002) at these P–T conditions would be only 0.28 ± 0.04 wt%.

To evaluate the amount of H_2O required in the analysed high-CO_2 BGB cordierite to enable it to be compatible with melting at the requisite P–T conditions, we have calculated the wt% H_2O in melts that would coexist with Opx + Sil + Qz + Feldspar at 11 kbar, 1000–1100 °C and specifically at 11.3 kbar/1050 °C. Calculations have been performed on a model NKFMASH bulk composition with X_{Mg} 0.88 and equivalent to Crd:Sil:Qz:Fsp in equal molar proportions (i.e., 1:1:1:1) using Theriak–Domino (de Capitani and Petrakakis 2010) and the Thermocalc dataset ds5.5 (Holland and Powell 2011). Calculations have also been carried out using Theriak–Domino with datasets ds5.5 and ds6 (White et al. 2014) on a similar composition with an additional 0.2 mol of An component, so that the resultant NCKFMASH bulk composition corresponds to the molar proportions Crd:Sil:Qz:Fsp of 1:1:1:1.2.

Figure 13 shows the phase relations calculated for the NKFMASH model bulk composition corresponding to Crd + Sil + Fsp + Qz in equal molar proportions (1:1:1:1),

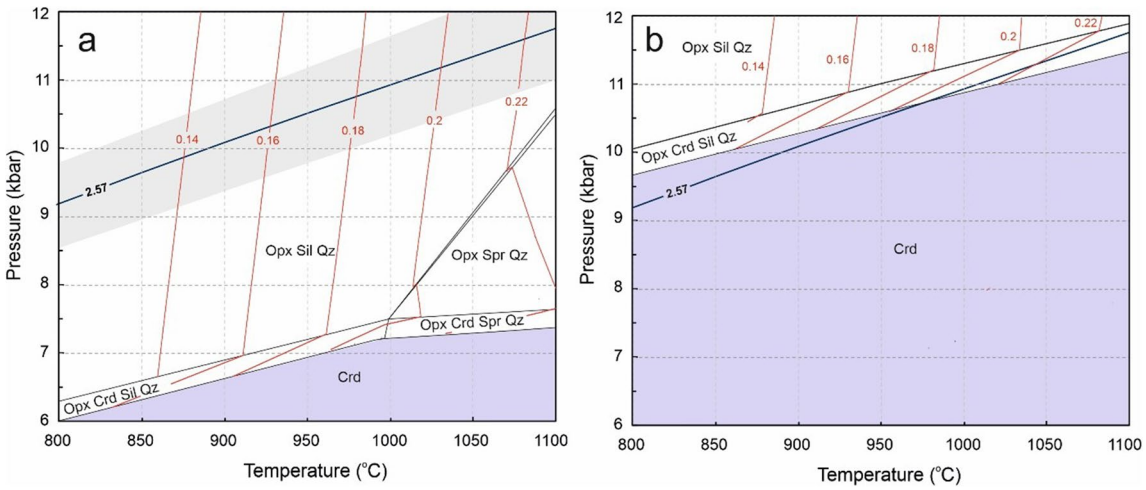

Fig. 12 **a** Stability of X_{Mg} 0.88 cordierite, on its own composition, in the FMAS system, calculated in Theriak–Domino (de Capitani and Petrakakis 2010) using Thermocalc dataset 5.5 (Holland and Powell 2011). The P–T position of the 2.57 wt% CO_2 isopleth in Bakhuis cordierite is from Fig. 11. **b** Stability of X_{Mg} 0.88 cordierite, on its own composition, in the FMASC system, modified from Fig. 12a to be in accord with the P–T position of the 2.57 wt% CO_2 isopleth in Bakhuis cordierite at 11.3 kbar and 1050 °C. In this semi-quantitative model, Opx + Sil + Qz forms at the expense of cordierite on cooling, producing Opx with X_{Al} of 0.2 at 1000 °C

with 0.05 mol pfu of H_2O added. Cordierite is not stable at the high P conditions modelled, as CO_2 is not accounted for in the datasets and modelling. Instead, the stable assemblage at 9–12 kbar and 1000–1050 °C is Opx + Sil + Kfs + Qz + L. The orthopyroxene in this assemblage at 1050 °C contains 10 wt% Al_2O_3 (X_{Al} = 0.205). This coexists with c. 5 vol% of melt containing c. 2 wt% H_2O, so that the model rock would be migmatitic and retain this amount of melt. The fields shown in this figure are metastable with respect to cordierite in the pure CO_2 system, for which the relevant assemblage at 11 kbar, 1050 °C would be Crd + Kfs, by comparison with Fig. 12.

The results of the Theriak–Domino calculations on melt generation for the model bulk compositions (Fig. 13) are summarised in Table 3. The essential result is that for temperatures of 1000–1050 °C (as suggested from ternary feldspar thermometry and the calculated phase diagrams of Appendix 1) and at pressures of ca. 11 kbar, melt would contain 2–3 wt% H_2O and reflect a_{H2O} conditions of 0.12–0.22. These estimates do not incorporate any corrections for CO_2, which can be present in the melts at high pressures, possibly at contents of up to 3000 ppm (0.3 wt%) based on D(CO_2) L/Crd values estimated by Harley (2008) [D = 0.1].

The Theriak–Domino calculations are compared in Table 3 with estimates produced using the Harley et al.'s (2002) modified calibrations for CO_2 and H_2O uptake in cordierite, on the assumption that the cordierite with high CO_2 is stabilised to 11.3 kbar at 1050 °C. Note that in the absence of CO_2, the low-H_2O cordierite consistent with a_{H2O} of 0.12–0.22 would not be stable at these P–T conditions: Opx + Sil + Qz would occur instead, as in the calculated phase diagrams produced for the CO_2-absent systems.

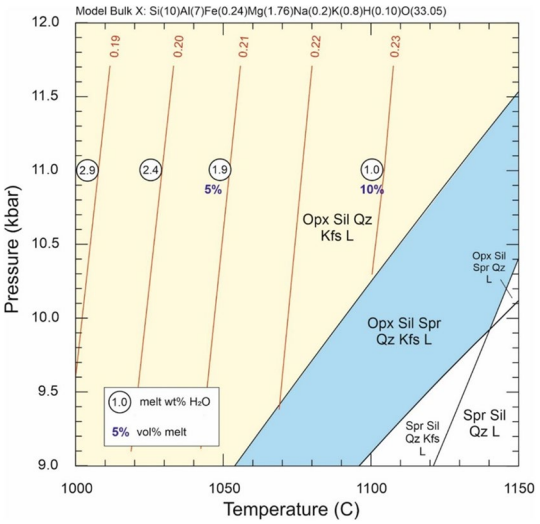

Fig. 13 Calculated phase diagram for the NKFMASH bulk composition with X_{Mg} 0.88 and equivalent to Crd:Sil:Qz:Fsp in equal molar proportions (i.e., 1:1:1:1). Model calculations performed using Theriak–Domino (de Capitani and Petrakakis 2010) and the Thermocalc dataset ds5.5 (Holland and Powell 2011). The bulk composition is almost dry, containing the molar equivalent of 0.083 wt% H_2O, selected to be consistent with the low measured H_2O content of cordierites in 71Sur210. 3–5 wt% granitic melt is produced in this model bulk composition at 11 kbar and 1000–1100 °C, containing 2.9–1.9 wt% H_2O and indicative of calculated a_{H2O} of 0.24–0.13. For cordierite to coexist with such a melt at these P–T conditions, it would need to contain some 1.2–0.9 wt% H_2O in addition to its high CO_2 (Table 3)

Table 3 also shows the H_2O contents that would be required to be present in peak CO_2-rich cordierite in order for the phase to be in equilibrium with the melts predicted

Table 3 Cordierite H_2O contents compatible with Theriak calculations

Model system, dataset, and cordierite to match model a_{H2O}	Cordierite parameters						Activities		Melt/Crd	H_2O	Theriak
	H_2O	CO_2	n(H_2O)	m(CO_2)	X_{CO2}crd	m + n	a_{CO2}	a_{H2O}	D_w	wt% melt	vol% melt
NKFMASH-tcds55											
Theriak								0.147		2.00	5.1
Cordierite	1.180	2.320	0.393	0.316	0.446	0.709	0.856	0.147	2.10	2.48	
CNKFMASH-tcds55											
Theriak								0.110		1.70	8.0
Cordierite	0.980	2.390	0.326	0.326	0.499	0.652	0.895	0.110	2.10	2.06	
CNKFMASH-tcds6											
Theriak								0.13		2.14	5.5
Cordierite	1.090	2.350	0.363	0.320	0.469	0.683	0.873	0.130	2.09	2.28	

Cordierite H_2O contents compatible with Theriak calculations based on Thermocalc datasets tcds55 and tcds6 at 11.3 kbar and 1050 °C for the NKFMASH bulk composition with X_{Mg} 0.88 and equivalent to Crd:Sil:Qz:Fsp in equal molar proportions (i.e., 1:1:1:1), modelled in Fig. 13, and a CNKFMASH bulk composition with 1:1:1 molar proportions of cordierite, sillimanite and quartz and a higher feldspar proportion (1.2 mol) to allow plagioclase and K-feldspar (or mesoperthite) to be present (Ca 0.2, Na 0.5, and K 0.5 molar proportions). Note the H_2O contents required of cordierite for it to be compatible (i.e., equivalent a_{H2O} at the given P–T) with the calculated melts in each case considered are greater than 1 wt%, significantly greater than all SIMS cordierite H_2O contents, including that of analysis C15 that was likely to have been affected by alteration or contamination

in Theriak, together with predicted melt wt% H_2O based on the Harley et al.'s (2002) methodology. At 11.3 kbar and 1050ºC, cordierite with c. 1.0–1.2 wt% H_2O yields appropriate a_{H2O} values, with the predicted melts having c. 2.0–2.5 wt% H_2O. These saturated cordierites would contain 2.32–2.39 wt% CO_2 and have channel X_{CO2} of 0.45–0.5 at the given P–T. These calculated CO_2 contents are in the lower range of values recorded in the Bakhuis cordierites, but do overlap with the CO_2 contents of three of the analyses in which H_2O is present at > 0.05 wt% (2.3–2.5 wt% CO_2). However, only in one of those analyses (C15 as noted in a previous section) is the H_2O content > 0.22 wt%, and even at c. 0.8 wt%, it is still well below that required for cordierite equilibrium with any sensible melt formed under the proposed P–T conditions. An a_{H2O} of 0.08 is calculated for this cordierite composition, leading to a predicted 'melt' H_2O of 1.7 wt%. This a_{H2O} is well below that required ($a_{H2O} = 0.12$) to stabilise a melt containing the minimum H_2O content of 2–2.5 wt% that is required based on the thermodynamic modelling.

Following from the calculations described above, there are three potential scenarios that could explain or resolve the paradox of having essentially H_2O-free cordierites present in migmatitic UHT granulite in the BGB. These are outlined below.

1. The high-CO_2 cordierites coexisted with low a_{H2O}, strongly H_2O-undersaturated melts at P > 11 kbar and T of 1050 °C but suffered near-peak H_2O loss from their channels, so that only CO_2 was retained. This interpretation would imply that, for most of the grains, some 1 wt% of H_2O was lost following the peak, during decompression or decompression-cooling at UHT. Back-calculating H_2O contents of 1.0–1.2 wt% into cordierite with 2.57 wt% CO_2 indicates that this amount of H_2O could be potentially be lost from cordierite on decompression through 700 bars (0.7 kbar) from 12 kbar, at 1050 °C, or on cooling through c. 80 °C, providing equilibrium was no longer maintained with melt. The governing factors on loss of H_2O in this instance are maintenance of fluid saturation coupled with melt loss. These two factors inexorably drive the cordierite to higher X_{CO2} through preferential loss (leakage) of the significantly more easily diffusible H_2O (e.g., Lepezin et al. 1995), whilst CO_2 remains constant and at or near saturation for the UHT P–T conditions preserved.
2. The high-CO_2 cordierites with negligible H_2O, and thus high-channel X_{CO2} (0.97), grew and equilibrated after melt extraction in an essentially H_2O-free residual rock composition. In this model, the cordierites never contained significant H_2O and were never in equilibrium with the low-a_{H2O} melts, which migrated to form the leucosomes observed in the migmatitic gneisses in the field. In this case, all the melting, and melt extraction took place prior to cordierite crystallisation. Hence, the migmatisation and melt redistribution, including melt loss, would be pre-peak.
3. The high-CO_2 cordierites cooled along a P–T trajectory parallel to the CO_2-H_2O saturation isopleths (2.57 wt% CO_2, 1.1 wt% H_2O; i.e., from 12/1050 °C to 8.7/700 °C on a dP/dT of 9.4 bar/ºC) and *then* underwent decompression and H_2O loss from cordierite at T far lower than those of UHT melting. Decompression through c. 0.7 kbar at 700 °C would be sufficient to remove the H_2O by 'leakage' in such a late-stage scenario, but may be kinetically less efficient than leakage under decompression/cooling at UHT.

The potential for H_2O loss from the CO_2-rich, volatile-saturated cordierites at or after UHT can be considered in the light of experimental diffusion and degassing kinetics studies conducted on cordierite (Lepezin and Melenevsky 1977; Lepezin et al. 1984, 1995; Jochum et al. 1983). Whilst in vacuo experiments by Lepezin and Melenevsky (1977) indicated that virtually all H_2O could be lost from a cordierite in a matter of days, the relevance of this to geological situations is not apparent. Of more relevance are the experiments of Lepezin et al. (1995), who determined the outgassing kinetics of cordierite for both H_2O and CO_2 based on 700–1000 °C experiments on two natural cordierites with differing X_{Mg} and initial CO_2/H_2O. The most significant result in this case was that H_2O was found to be lost from cordierite at a rate 1000 times faster than CO_2, at T < 700 °C, allowing the possibility that post-UHT preferential loss of H_2O (scenario 3 above) could be plausible. However, none of the experimental degassing data are directly applicable to cordierites initially formed at c. 11 kbar and 1050 °C and then allowed to cool and decompress to lower temperatures still at 7–8 kbar, and the blocking effects of cations (e.g., Na, K, Li: Jochum et al 1983) in the channel sites remain poorly quantified.

In summary, there is currently no reliable experimental basis on which to select from the three alternatives described above—all three remain open possibilities. In view of this, and to highlight the uniqueness of the Bakhuis cordierite example, we now consider other natural examples of CO_2-rich cordierite in typical migmatitic granulites and UHT rocks.

Other high-CO_2 cordierites and their implications for the BGB UHT cordierite

The highest CO_2 cordierite hitherto recorded in nature is that from a cordierite–calcite–pyrite 'reaction rock' from Valjok in the Norwegian part of the Lapland granulite belt, described in detail by Armbruster et al. (1982). The

cordierite occurs in patches within otherwise cordierite-free and non-foliated Grt + Sil + Bt + Opx + Plag + Qz reaction rock seams or dykes that cut foliated gneisses. With CO_2 contents of 2.2 wt% and H_2O at 0.3 wt% the Lapland cordierite has X_{CO2} of 0.75 and is compatible with fluid saturation and an a_{CO2} of 0.98 at 8.5 kbar and 850 °C (Table 4), the peak P–T conditions previously inferred for the granulite belt. Given the discordant nature of the host reaction rock, it is possible that they and the high-CO_2 cordierite were generated subsequent to peak granulite metamorphism, at lower P–T. If that were the case, the relevant saturation isopleth for this cordierite combined with the stability of sillimanite in the reaction rock indicates that it may have formed at P–T as low as 6.9 kbar and 650 °C. This highly unusual cordierite occurrence is not comparable to the Bakhuis case, which in terms of mineral assemblage and textural context bears more similarity to cordierites in migmatitic metapelitic and metasemipelitic granulites, considered below.

Whilst CO_2-bearing cordierite is relatively common in cordierite-bearing migmatitic granulite metapelites and metasemipelites formed under P–T conditions of 5–8 kbar and 750–900 °C, the vast majority contain less than 0.8 wt% CO_2 (Harley et al. 2002; Harley and Thompson 2004; Rigby and Droop 2008). A small number have higher CO_2 contents, but these rarely exceed 1.6 wt% (Vry et al. 1990; Harley et al. 2002; Harley and Thompson 2004; Table 4). Irrespective of their CO_2 contents, these cordierites are generally present as porphyroblastic or matrix phases in association with Bt + Grt + Qz + Feldspars (lower T < 800 °C), Opx + Grt + Qz + Feldspars (> 800 °C) or Grt + Sil + Qz + Feldspars (+ Bt). The cordierites generally contain between 0.3 and 1 wt% H_2O, have channel X_{CO2} of < 0.6 and are usually fluid-undersaturated at the inferred P–T conditions of peak metamorphism (Table 4). For example, high-CO_2 cordierite 8/90 (1.3 wt% CO_2, 0.8 wt% H_2O) from migmatitic metapelite of the Serre Massif in Calabria (Schenk et al. 1993) has X_{CO2} of 0.4 and implies total fluid activity (0.73) much less than unity at the peak P–T. In common with most other examples of migmatite cordierite, melt H_2O contents calculated from the H_2O content of this cordierite using the D_w relations of Harley and Carrington (2001) are c. 1.7–1.9 wt%. These calculated melt H_2O contents, somewhat lower than those appropriate to granulite temperatures of c. 850 °C (2.5 wt%), have been interpreted in terms of partial H_2O leakage or loss from cordierite on post-peak decompression with cooling (e.g., Harley and Thompson 2004; Rigby and Droop 2008). However, even when H_2O is added back into the cordierite to bring it into equilibrium with melt at 850 °C (Crd H_2O = 1 wt%), the cordierite is still volatile-undersaturated (total fluid activity = 0.78), consistent with fluid-undersaturated, melt-present, conditions.

Although most granulite–facies cordierites are volatile-undersaturated at peak P–T, and may have suffered partial post-peak H_2O loss in a number of cases (Rigby and Droop 2008), a small group that contain c. 1.6 to 1.9 wt% CO_2 appear to record volatile saturation at or near-peak P–T conditions (Table 4). For example, cordierite in sample 15/81, a pelite from the Serre Massif (Schenk et al 1993), contains 1.90 wt% CO_2, resulting in a calculated a_{CO2} of 0.95 at 7.8 kbar and 860 °C. High-CO_2 cordierite from Cauchon Lake in the Pikwitonei granulite terrane (Vry et al. 1990) likewise is saturated at the inferred peak P–T of 7.2 kbar and 775 °C, and implies a_{CO2} of 0.97. Whilst both of these cordierite examples contain H_2O, the preserved concentrations (0.33–0.55 wt% H_2O) when coupled with D_w relationships again yield apparent melt H_2O contents of 1.0–1.5 wt%—too low for granitic melt at 775–900 °C (3.0–2.0 wt%). The implication is that either melt was absent from these particular granulites when cordierite crystallised or that the cordierites formed at slightly higher P, in the presence of melt, and then lost some H_2O on their post-peak P–T evolution. As with the lower CO_2 examples discussed above, it is notable that any loss of H_2O from the cordierites following peak crystallisation has only been partial: there are no examples of cordierite from migmatitic granulites that can be shown to have entirely lost all of the H_2O that may be expected to have been contained in them on crystallisation from or with melt.

The final mode of occurrence of CO_2-rich cordierite in granulites that is relevant to this discussion is its presence in post-peak reaction coronas in UHT metapelites and metaquartzites (Table 4). Such coronal cordierite may occur on reactant sapphirine + quartz (Spr + Qz), as at Mount Hardy in the Napier Complex (Harley 2008), on Opx + Sil + Qz, as in the Arequipa Complex of Peru (Martignole and Martelat 2003), and with sapphirine on Grt + Sil, as in the Anapolis Complex of Brazil (Baldwin et al. 2005; Harley 2008). The highest-CO_2 example of such post-peak UHT cordierite is that from Anapolis, which contains 1.45 wt% CO_2 as well as considerable H_2O (0.78 wt%). This coronal cordierite is fluid-saturated at c. 7.9 kbar and 950–1000 °C (Table 4), and is considered to have formed due to localised fluid access on cooling following peak UHT metamorphism (e.g., Baldwin et al. 2005). In this case the infiltrating fluid was not simply CO_2 but CO_2–H_2O fluid with a_{CO2} of 0.79. In the case of Arequipa, the coronal cordierite preserves 1 wt% H_2O along with 1.05 wt% CO_2 and thus has a channel X_{CO2} of 0.3 and associated a_{CO2} of 0.47. This cordierite, which is strongly volatile-undersaturated (a_{fluid} (total) = 0.64), may have formed through reaction of the Opx + Sil + Qz with residual melt at 8 kbar/920–900 °C rather than by external fluid infiltration (Harley 2008). Coronal cordierite from Mount Hardy in the Napier Complex (Table 4) has very similar CO_2 to the Arequipa example but much lower H_2O (0.22 wt%), and is

strongly volatile-undersaturated ($a_{fluid} = 0.57$). Adding H_2O back into this cordierite to allow it to coexist with a melt containing 1.7 wt% H_2O at 7.5 kbar and 950C (Harley and Thompson 2004) gives a H_2O content of only 0.45 wt%, and a_{fluid} (0.61) that still indicates strongly fluid-undersaturated, melt-present, conditions for post-peak UHT corona formation. In all, these UHT examples support the conclusions drawn from the migmatitic granulites that the formation of moderately high-CO_2 cordierite does not require fluid saturation and that, in general, H_2O leakage from such cordierite ranges from negligible to moderate and is never total, in line with the observations of Rigby and Droop (2008).

From the evidence provided above, it is clear that the BGB CO_2-rich cordierite is unique in its following:

(a) Preservation of the highest CO_2 contents yet recorded, c. 2.57 wt%;
(b) Lack of H_2O, so that X_{CO2} of the cordierite is near unity, notably higher even than the Valjok Lapland cordierite of Armbruster et al. (1982);
(c) Occurrence as a peak- or near-peak porphyroblastic phase formed under UHT conditions in equilibrium with Sil + Mesoperthite ± Opx + Qz, and
(d) Being fluid saturated for all feasible granulite P–T conditions.

Furthermore, unless all H_2O leaked out of its channels, this cordierite cannot have been in equilibrium with melt at c. 11 kbar and 1000–1100 °C or indeed at any other lower pressure. By comparison with all other CO_2-bearing cordierites in metapelitic and migmatitic granulites and indeed with cordierites developed in UHT coronas, all of which retain H_2O contents of 0.2–1.0 wt%, such total and complete H_2O loss is highly unlikely.

If total H_2O loss is highly unlikely for the CO_2-rich BGB cordierite, this would imply that the cordierite did not form during the main phase of UHT melting and migmatization, but after the migmatization. However, even then the formation of the CO_2-rich cordierite would require a considerable amount of CO_2. Based on the ternary feldspar temperatures determined by Nanne et al. (2020), melting occurred under UHT conditions. The common presence of CO_2-rich fluid inclusions in the solidified melts would imply that there was a considerable amount of CO_2 present during the peak UHT stage with melting. This, combined with the common presence of cordierite in leucosomes and the absence of evidence for an older leucosome assemblage being replaced by the cordierite, would make it highly unlikely that the CO_2-rich cordierite was formed at a later stage of UHTM and not during the peak stage with melting. Total H_2O loss from the CO_2-rich cordierite is unlikely, but not impossible. If one has to choose from two unlikely scenarios, cordierite formation during the peak UHT stage with melting is preferred. SIMS analysis of other BGB cordierites might show the same total loss of H_2O if that loss was caused by the long UHTM and the complex exhumation of the BGB. Raman microspectroscopy did not show H_2O in the SIMS analysed cordierite in sample 71Sur210. However, it showed some H_2O for another blue birefringent cordierite, suggesting a less than total H_2O loss.

Peak to near-peak P–T fluid saturation in the BGB

The presence of primary cordierite with a high CO_2 content in migmatitic granulites does not of itself necessarily imply the presence of a free carbonic fluid phase in addition to melt at peak granulite/UHT P–T conditions (Harley 2008). However, if fluid inclusions are observed in porphyroblastic phases in such cordierite-bearing migmatites, it is almost certain that a free fluid phase became present at some stage of their high-T melt-bearing evolution (Harley and Thompson 2004). Fluid inclusions (FI) are present in quartz and feldspar in the leucosomes of Bakhuis metapelites and intermediate granulites, assumed to have formed during crystallisation of the partial melt produced at or near-peak UHT conditions. The FI show the high relief characteristic of CO_2-rich compositions, and the presence of CO_2 has been proven for 11 samples subjected to C^{13}/C^{12} analysis (Donker 2021). One of the samples was used as reference by Luciani et al. (2022), they found only CO_2 in the FI by Raman microspectroscopy. The evidence for peak- or near-peak CO_2 fluid inclusions, along with the presence of volatile-saturated, extremely high-CO_2 cordierite in migmatitic and quartzitic UHT granulites in the BGB, strongly points to the presence of a CO_2-dominant fluid at or near the metamorphic peak in this deep-seated and unusual UHT terrain.

Internal or external CO_2 source for the formation of CO_2-rich cordierite in the BGB

The formation of fluid-saturated CO_2-rich cordierite on a regional scale requires the presence of considerable volumes of fluid. In the case of the BGB, if the two cordierite-bearing quartzites (~ 20 vol% cordierite with c. 2.6 wt% CO_2) are representative of the more widespread cordierite-bearing migmatites, then around 0.5 wt% CO_2 would be required to achieve fluid saturation in any given metapelite rock volume. A local source of CO_2 may be provided through decarbonation of calcareous rocks, but in the BGB, the metapelites are accompanied only locally by calcareous rocks (now Ca-silicate granulites), and in small amounts. Ca-silicate granulites form one of the dominant rock types only in the K3 area in the southwest of the BGB (Fig. 2), whereas metapelites with highly birefringent cordierite occur at the margins of this area but also far removed from this area (Fig. 10).

Table 4 Selected cordierite volatile content data and fluid activity calculations for 'normal' and UHT granulites

Sample and reference	P (kbar)	T (°C)	Cordierite volatile compositions						Activities (Crd)			Melt/Crd	Melt	Notes
			H_2O	CO_2	n(H_2O)	m(CO_2)	m + n	X_{CO2}crd	a_{H2O}	a_{CO2}	a_{fluid}	D_w	wt% H_2O	
Normal Granulites (< 900 °C)														
Sturbridge, Massachusetts (1)	6.3	730	0.56	1.37	0.188	0.188	0.376	0.50	0.07	0.71	0.79	2.46	1.38	
Wind River Wyoming (1)	6.4	750	0.58	1.67	0.197	0.232	0.429	0.54	0.08	0.94	1.02	2.92	1.69	Saturated
Manivitsy, Madagascar (1)	7	850	0.60	1.31	0.201	0.180	0.381	0.47	0.09	0.69	0.78	2.83	1.70	
Southern Madagascar (1)	7	850	0.74	1.49	0.248	0.205	0.453	0.45	0.12	0.81	0.93	2.72	2.01	
Pikwitonei, Cauchon (1)	7.2	775	0.59	1.94	0.198	0.266	0.465	0.57	0.07	0.97	1.04	2.56	1.51	Saturated
Pikwitonei, Cauchon (1)	7.2	775	0.60	1.58	0.201	0.217	0.418	0.52	0.07	0.74	0.81	2.55	1.53	
Pikwitonei, Prud'homme (1)	7.2	800	0.33	1.52	0.111	0.209	0.320	0.65	0.04	0.73	0.77	3.18	1.05	
Serre, Calabria 8/90 (2)	7.5	850	0.80	1.30	0.270	0.180	0.450	0.40	0.10	0.57	0.67	2.40	1.92	
Serre, Calabria 15/90 (2)	7.8	860	0.33	1.90	0.111	0.262	0.374	0.70	0.04	0.95	0.99	3.19	1.05	Saturated
Arendal (1)	9	800	1.04	1.61	0.349	0.221	0.570	0.39	0.11	0.54	0.65	1.92	2.00	
Post-granulite reaction rock														
Norwegian Lapland (3)	8.5	850	0.30	2.20	0.100	0.301	0.401	0.75	0.03	0.98	1.01	2.95	0.89	Saturated
UHT Granulites														
Anapolis, Brazil (4)	7.9	1000	0.87	1.45	0.291	0.198	0.489	0.41	0.17	0.79	0.96	3.02	2.63	Saturated, corona
Mount Hardy, Napier (5)	7.5	950	0.22	1.04	0.071	0.141	0.213	0.66	0.03	0.54	0.57	4.35	0.94	Corona
Arequipa, Peru (4)	8	920	1.00	1.05	0.336	0.144	0.480	0.30	0.17	0.47	0.64	2.63	2.63	Corona

In the case of typical or normal granulites, the data have been selected to include only those high-CO_2 cordierites with a minimum of 1.3 wt% CO_2. The minimum CO_2 criterion applied to UHT granulites in which cordierite occurs in coronas is 1.0 wt% CO_2. The post-peak granulite reaction rock from Valjok in Norwegian Lapland (Armbruster et al. (1982) is distinguished as the only other cordierite with > 2 wt% CO_2

References: (1) Vry et al. (1990); (2) Schenk et al. (1993); (3) Armbruster et al. (1982); (4) Harley (2008); (5) Harley and Thompson (2004)

In the absence of a major local source, an external CO_2 source is required, such as that potentially provided on a regional scale by asthenospheric upwelling and/or mafic underplating, as suggested by Delor et al. (2003), Klaver et al. (2015), and Beunk et al. (2021) to explain the heat source required for UHT metamorphism of the BGB. Whilst large mafic–ultramafic intrusions are abundant in the SW part of the BGB, they are ~ 70 Ma younger than the UHT metamorphism (Klaver et al. 2016). Narrow high-grade metadolerite dykes have been formed and subsequently deformed during UHTM (De Roever et al. 2019; 2022). They have a characteristic MgO-rich composition, with up to 15% MgO. The deformed dykes form clear evidence for mafic magmatism co-eval with UHTM, but the dykes are too small to represent the UHTM heat source (De Roever et al. op. cit.). However, the magmatism may have been more extensive at greater depth.

Direct evidence for the source of the CO_2 is provided by the $\delta^{13}C$ value of -4.5 ± 0.8 determined by Luciani et al. (2022) for CO_2 in fluid inclusions in quartz in granulite from Blanche Marie Falls, in the core of the BGB. They conclude that this composition is in accordance with CO_2-rich fluids released by mantle-derived magmas.

An external CO_2 source for the formation of CO_2-rich cordierite ± free carbonic fluid under UHT conditions (possibly from the mantle) would explain the rarity of UHT occurrences with widespread primary CO_2-rich cordierite. Among the ~ 70 UHT occurrences worldwide (Harley 2020; Kelsey and Hand 2015), the BGB is the only occurrence with such cordierite. However, the matter of the source of CO_2 in the BGB cordierite cannot be resolved without further investigation of the high-CO_2 cordierites from several migmatitic metapelites in the BGB and analysis of their $\delta^{13}C$ isotopic compositions, which is beyond the scope of the present study.

Conclusions

1. SIMS analysis has revealed that blue birefringent cordierite in a metapelitic granulite from the BGB contains c. 2.6 wt% CO_2 and negligible H_2O. The measured CO_2 is the highest level found for any natural cordierite.
2. Modelling of the uptake of CO_2 by cordierite as a function of P, T, and a_{CO2} based on a revised version of Harley et al. (2002) leads to calculated pressures of 11.3 kbar at 1050 °C for the UHT formation and equilibration of the near-pure CO_2 cordierite at a_{CO2} of c. 1.0. The P–T conditions overlap with those deduced from Opx + Sil + Qz assemblages in the BGB (and a garnet granulite) and are compatible with experimental constraints on the stability of cordierite in the presence of CO_2 and mixed H_2O–CO_2 fluids.
3. The extremely low H_2O contents of the best-preserved cordierite grains (0.037 wt%) in the analysed sample yield a very low calculated a_{H2O} (0.003) that is incompatible with melting in the metapelite even under the extreme P–T conditions proposed for this UHT terrain.
4. Whilst H_2O leakage or preferential diffusional loss from the studied cordierite is possible, it is considered unlikely, given the commonly observed presence of H_2O in all other natural cordierites, that the negligible H_2O contents reflect near-total H_2O loss from this UHT cordierite. An alternative might be that the near-pure CO_2 cordierite in the metapelite was formed after migmatization and melting.
5. The presence of abundant metapelitic and metasemipelitic migmatite in the BGB attests to significant melting under the ambient UHT conditions. More highly birefringent cordierites present in those rocks, from other sites in the BGB, should be subjected to volatiles analysis.
6. The source for the CO_2 in the analysed metapelitic cordierite, and more generally in the cordierites from across the BGB, is not constrained but is likely to be external, and perhaps mantle-derived, given the regional scale of cordierite occurrence and the paucity of carbonate lithologies. This proposal requires assessment through a detailed $\delta^{13}C$ isotopic study of the BGB cordierites in parallel with additional volatile measurements noted in conclusion 5.

Supplementary Information The online version contains supplementary material available at https://doi.org/10.1007/s00410-023-02003-1.

Acknowledgements EdR is indebted to the Dutch Dr. Schürmann Foundation for Precambrian research (www.dr-schuermannfonds.nl) for generous financial support for all his expeditions and field work in the BGB since 2005 (e.g., Grants 38/2006, 70/2010, 90B/2015, 107/2015). The Dutch Molengraaff Foundation is thanked for travel subsidies to MSc-students participating in the field work. The (then) M.Sc. students R.A. de Boer, R.S. Donker, K. de Groot, M. Klaver, W. van de Steeg, A.C.D. Thijssen, B. Uunk, H. C. Vos, and in particular J.A.M. Nanne are thanked for their contributions to this article. Wim Lustenhouwer and Dr. Sergei Matveev made the electron-microprobe analyses of cordierite at Vrije Universiteit Amsterdam, while M.J.C. Bouten is thanked for analyses with the JEOL JXA 8530F at the Laboratory for Micro-analysis at Utrecht. The Edinburgh Ion Microprobe Facility (EIMF) is thanked for providing access to the ims4f ion microprobe and assistance with its analytical set-up. The National History Museum Naturalis at Leiden and the Geological and Mining Service of Surinam (GMD) are thanked for the borrowing of samples. The director of the GMD and his staff are thanked for access to maps, reports and samples. Special thanks are due to Karel and Joyce Dawson of the Kabalebo Nature Resort and the Resort staff, for their generous support and assistance. Thanks to Norman McIntosh for his great support and energy during his FWD expeditions with me into the BGB. Prof. Dr. H.N.A. Priem helped by taking the cordierite-bearing sample 71Sur210 on his geochronology expedition in the BGB. Tim Johnson and an unknown reviewer are thanked for their constructive comments.

Data availability All analytical data and calculated data required for this study are included within the article or the supplementary data file.

Declarations

Conflict of interest The authors have no financial or proprietary interests in any material discussed in this article.

References

Ague JJ (2012) Precipitation of rutile and ilmenite needles in garnet: Implications for extreme metamorphic conditions in the Acadian Orogen, USA. Am Miner 97:840–855

Armbruster Th, Bloss FD (1980) Channel CO_2 in cordierites. Nature 286:140–141

Armbruster Th, Schreyer W, Hoefs J (1982) Very high CO_2 cordierite from Norwegian Lapland. mineralogy, petrology and carbon isotopes. Contrib Miner Petrol 81:262–267

Armstrong JT (1988) Quantitative analysis of silicate and oxide materials: Comparison of Monte Carlo, ZAP, and φ(ρz)) procedures. In: Newbury E (ed) Microbeam analysis. San Francisco Press, pp 239–246

Baldwin JA, Powell R, Brown M, Moraes R, Fuck RA (2005) Modelling of mineral equilibria in ultrahigh-temperature metamorphic rocks from the Anápolis-Itauçu Complex, central Brazil. J Metamorph Geol 23:511–531

Bebout GE, Lazzeri KE, Geiger CA (2016) Pathways for nitrogen cycling in Earth's crust and upper mantle: a review and new results for microporous beryl and cordierite. Am Miner 101:7–24

Bertrand P, Ellis DJ, Green DH (1991) The stability of sapphirine-quartz and hypersthene-sillimanite-quartz assemblages: an experimental investigation in the system FeO-MgO-Al_2O_3-SiO_2 under H_2O and CO_2 conditions. Contrib Min Petrol 108:55–71

Beunk FF, de Roever EWF, Yi K, Brouwer FM (2021) Structural and tectonothermal evolution of the ultrahigh-temperature Bakhuis Granulite Belt, Guiana Shield, Surinam: Paleoproterozoic to recent. Geosci Front 12:677–692

de Capitani C, Petrakakis K (2010) The computation of equilibrium assemblage diagrams with Theriak/Domino software. Am Miner 95:1006–1016

De Roever EWF, Lafon JM, Delor C, Cocherie A, Rossi P, Guerrot C, Potrel A (2003) The Bakhuis ultrahigh-temperature granulite belt (Suriname): I. Petrological and geochronological evidence for a counter-clockwise P-T path at 2.07–2.05 Ga. Geologie De La France (BRGM) 2003 Revue 2:175–205

De Roever EWF, Beunk FF, Yi K, De Groot, K, Klaver M, Nanne JAM, van de Steeg W, Thijssen ACD, Uunk B, Vos H, Davies GR, Brouwer FM (2019) The Bakhuis granulite belt in W Suriname, its development and exhumation. 11th Inter-Guiana Geological Conference: Tectonics and Metallogenesis of NE South America. Paramaribo, Suriname, 2019. Also: Extended Abstract in Mededeling Geol. Mijnbouwkd. Dienst Suriname 29, 53–58

De Roever E, Beunk F, Yi K, Donker R-J, van de Steeg W, Uunk B, Davies GR, Brouwer FM (2022) Ultrahigh-temperature metamorphism in the Bakhuis Granulite Belt (Surinam). XII Inter Guiana Geological Conference 2022, Georgetown, Guyana. Extended Abstract in Proceedings p. 54–58

Deer WA, Howie RA, Zussmann J (1997) Rock-forming minerals. Part 1B, disilicates and ring silicates, 2nd edn. The Geological Society, London

Delor C, De Roever EWF, Lafon JM, Lahondère D, Rossi P, Cocherie A, Guerrot C, Potrel A (2003) The Bakhuis ultrahigh-temperature granulite belt (Suriname): II. Implications for late Transamazonian crustal stretching in a revised Guiana Shield framework. Géologie De La France (BRGM) 2003 Revue 2:207–230

Donker RS (2021) On the origin of CO2 inclusions in ultrahigh-temperature metamorphic rocks from the Bakhuis Granulite Belt, western Surinam. MSc. Thesis. Vrije Universiteit Amsterdam. p. 1–79

Fitzsimons ICW, Mattey DP (1995) Carbon isotope constraints on volatile mixing and melt transport in granulite-facies migmatites. Earth Planet Sci Lett 134:319–328

Gou L, Zhang C, Zhang L, Wang Q (2014) Precipitation of rutile needles in garnet from sillimanite-bearing pelitic granulite from the Khondalite Belt North China Craton. Chin Sci Bull 59(32):4359–4366

Harley SL (1998) On the occurrence and characterization of ultrahigh-temperature crustal metamorphism. In: Treloar PJ, O'Brien PJ (eds) What drives metamorphism and metamorphic reactions? Geological Society, vol 138. Special publication, London, pp 81–107

Harley SL (2008) Refining the P-T records of UHT crustal metamorphism. J Metamorph Geol 26:125–154

Harley SL (2020) UHT metamorphism. In: Alderton D, Elias SA (eds) Encyclopedia of geology, 2nd edn. Academic Press (Elsevier), Cambridge

Harley SL, Carrington DP (2001) The distribution of H_2O between cordierite and granitic melt: H_2O incorporation in cordierite and its application to high-grade metamorphism and crustal anatexis. J Petrol 42:1595–1620

Harley SL, Green DH (1982) Garnet-orthopyroxene barometry for granulites and peridotites. Nature 300:697–701

Harley SL, Thompson P (2004). The influence of cordierite on melting and mineral-melt equilibria in ultra-high-temperature metamorphism. Fifth Hutton Symposium: The Origin of Granites and Related Rocks, Geological Society America Special Papers 389, p. 87-98

Harley SL, Thompson P, Hensen BJ, Buick IS (2002) Cordierite as a sensor of fluid conditions in high-grade metamorphism and crustal anatexis. J Metamorph Geol 20:71–86

Hensen BJ, Harley SL (1990) Graphical analysis of P-T–X relations in granulite facies metapelites. In: Ashworth JR, Brown M (eds) High Temperature Metamorphism and Crustal Anatexis. Unwin Hyman, London, pp 19–56

Holland TJB, Powell R (2011) An improved and extended internally consistent thermodynamic dataset for phases of petrological interest, involving a new equation of state for solids. J Metamorph Geol 29:333–383

Jochum C, Mirwald PW, Maresch W, Schreyer W (1983) The kinetics of H_2O exchange between cordierite and fluid during retrogression. Fortschr Miner 61:103–105

Johannes W, Schreyer W (1981) Experimental introduction of CO_2 and H_2O into Mg-cordierite. Am J Sci 281:299–317

Kaindl R, Tropper P, Deibl I (2006) A semi-quantitative technique for determination of CO_2 in cordierite by Raman spectroscopy in thin sections. Eur J Miner 18:331–335

Keller DS, Ague JJ (2019) Crystallographic and textural evidence for precipitation of rutile, ilmenite, corundum, and apatite lamellae from garnet. Am Miner 104:980–995

Kelsey DE, Hand M (2015) On ultrahigh temperature crustal metamorphism: phase equilibria, trace element thermometry, bulk composition, heat sources, timescales and tectonic settings. Geosci Front 6:311–356

Klaver M, de Roever EWF, Nanne JAM, Mason PRD, Davies GR (2015) Charnockites and UHT metamorphism in the Bakhuis Granulite Belt, western Suriname: evidence for two separate UHT events. Precambr Res 262:1–19

Klaver M, de Roever EWF, Thijssen ACD, Bleeker W, Soderlund U, Chamberlain K, Ernst R, Berndt J, Zeh A (2016) Mafic magmatism in the Bakhuis Granulite Belt (western Suriname): relationship with charnockite magmatism and UHT metamorphism. GFF 138:203–218

Kroonenberg SB, de Roever EWF, Fraga LM, Reis NJ, Faraco T, Lafon J-M, Cordani U, Wong TE (2016) Paleoproterozoic evolution of the Guiana Shield in Suriname: a revised model. Neth J Geosci 95–4:491–522

Kurepin VA (1985) H_2O and CO_2 contents of cordierite as an indicator of thermodynamical conditions of formation. Geochem Int 22:148–156

Kurepin VA (2010) Cordierite as an indicator of thermodynamic conditions of petrogenesis. Contrib Miner Petrol 160:391–406

Le Breton N, Schreyer W (1993) Experimental CO_2 incorporation in Mg-cordierite: non-linear behaviour of the system. Eur J Miner 5:427–438

Lepezin G, Melenevsky VN (1977) On the problem of water diffusion in cordierites. Lithos 10:49–57

Lepezin G, Osorgin NYu, Shvedenkov GYu (1984) Determination of the diffusion coefficients of CO_2 in cordierites. Doklady Rossiyskoy Akademii Nauk 275:970–974

Lepezin G, Osorgin NYu, Shvedenkov GYu (1995) Natural cordierite outgassing kinetics: determination of CO_2 diffusion coefficient under isothermal conditions. Doklady Rossiyskoy Akademii Nauk 342:92–94

Luciani N, van der Lubbe JHL, Verdegaal-Warmerdam SJA, Postma O, Nikogosian IK, Davies GR, Koornneef JM (2022) Carbon and oxygen analysis of CO_2 trapped in silicate minerals. Chem Geol 602:120872

Martignole J, Martelat J-E (2003) Regional-scale Grenvillian-age UHT metamorphism in the Mollendo-Camana block (basement of the Peruvian Andes). J Metamorph Geol 21:99–120

Muir ID (1967) Chapter 2 of Physical methods in determinative Mineralogy. In: Zussmann J (ed) Microscopy: transmitted light. Academic Press, London

Nanne JAM, de Roever EWF, de Groot K, Davies GR, Brouwer FM (2020) Regional UHT metamorphism with widespread, primary CO_2-rich cordierite in the Bakhuis Granulite Belt, Surinam: a feldspar thermometry study. Precambr Res 350:105894

Nesse WD (2000) Introduction to mineralogy. Oxford University Press, New York

Rigby MJ, Droop GTR (2008) The cordierite fluid monitor: case studies for and against its potential application. Eur J Mineral 20:693–712

Schenk V, Herms P, Le Breton P, Craven J, Harley SL (1993) Cordierite as a fluid indicator in metamorphic rocks (abstract). Terra Abstracts Supplement Terra Nova 5:467

Tateishi K, Tsunogae T, Santosh M, Janardhan AS (2004) First report of sapphirine quartz assemblage from Southern India: implications for ultrahigh-temperature metamorphism. Gondwana Res 7:899–912

Thompson P, Harley SL, Carrington DP (2001) The distribution of H_2O-CO_2 between cordierite and granitic melt under fluid-saturated conditions at 5 kbar and 900°C. Contrib Miner Petrol 142:107–118

Touret JLR, Santosh M, Huizenga JM (2016) High-temperature granulites and supercontinents. Geosci Front 7:101–113

Vos H (2016) The origin of the mafic and intermediate granulites in the Bakhuis Granulite Belt, West Suriname. MSc thesis. Vrije Universiteit Amsterdam. p. 1–124

Vry JK, Brown PE, Valley JW (1990) Cordierite volatile content and the role of CO_2 in high-grade metamorphism. Am Miner 75:71–88

White RW, Powell R, Holland TJB, Johnson TE, Green ECR (2014) New mineral activity-composition relations for thermodynamic calculations in metapelitic systems. J Metamorph Geol 32:261–286

Whitney DL, Evans BW (2010) Abbreviations for names of rock-forming minerals. Am Miner 95:185–187

Wu C-M (2019) Original calibration of a garnet geobarometer in metapelite. Minerals 9(9):540–553. https://doi.org/10.3390/min9090540